NIH Public Access
Author Manuscript
Hippocampus. Author manuscript; available in PMC 2013 August 01.

Published in final edited form as:
Hippocampus. 2012 August ; 22(8): 1659–1680. doi:10.1002/hipo.22002.

Activity Dynamics and Behavioral Correlates of CA3 and CA1 Hippocampal Pyramidal Neurons

Kenji Mizuseki[1], **Sebastien Royer**[1,2], **Kamran Diba**[1], and **György Buzsáki**[1,2]

[1]Center for Molecular and Behavioral Neuroscience, Rutgers, The State University of New Jersey, Newark, New Jersey

[2]Howard Hughes Medical Institute, Janelia Farm Research Campus, Ashburn, Virginia

Abstract

The CA3 and CA1 pyramidal neurons are the major principal cell types of the hippocampus proper. The strongly recurrent collateral system of CA3 cells and the largely parallel-organized CA1 neurons suggest that these regions perform distinct computations. However, a comprehensive comparison between CA1 and CA3 pyramidal cells in terms of firing properties, network dynamics, and behavioral correlations is sparse in the intact animal. We performed large-scale recordings in the dorsal hippocampus of rats to quantify the similarities and differences between CA1 (n > 3,600) and CA3 (n > 2,200) pyramidal cells during sleep and exploration in multiple environments. CA1 and CA3 neurons differed significantly in firing rates, spike burst propensity, spike entrainment by the theta rhythm, and other aspects of spiking dynamics in a brain state-dependent manner. A smaller proportion of CA3 than CA1 cells displayed prominent place fields, but place fields of CA3 neurons were more compact, more stable, and carried more spatial information per spike than those of CA1 pyramidal cells. Several other features of the two cell types were specific to the testing environment. CA3 neurons showed less pronounced phase precession and a weaker position versus spike-phase relationship than CA1 cells. Our findings suggest that these distinct activity dynamics of CA1 and CA3 pyramidal cells support their distinct computational roles.

Keywords

network dynamics; bursts; place cells; phase precession; firing rates

INTRODUCTION

A large body of experimental findings supports the role of the hippocampus in spatial navigation and episodic memory (O'Keefe and Nadel, 1978; Squire, 1992; O'Keefe and Recce, 1993; Eichenbaum et al., 1999; McNaughton et al., 2006; Pastalkova et al., 2008). The hippocampus consists of two major regions, the strongly recurrent network of CA3 pyramidal cells and the largely parallel-organized or feed-forward network of the CA1 region (Amaral and Witter, 1989; Amaral and Levenex, 2007). These fundamental structural differences between the two regions suggest distinct computational roles (McNaughton and

© 2012 WILEY PERIODICALS, INC.

*Correspondence to: György Buzsáki, Center for Molecular and Behavioral Neuroscience, Rutgers University, 197 University Avenue, Newark, NJ 07102, USA. buzsaki@axon.rutgers.edu.
Sebastien Royer is currently at Center for Functional Connectomics, KIST 39-1 Hawolgokdong, Seongbukgu, Seoul, Republic of Korea 136–791.
Kamran Diba is currently at Department of Psychology, University of Wisconsin at Milwaukee, Milwaukee, Wisconsin 53211.

NIH-PA Author Manuscript
NIH-PA Author Manuscript
NIH-PA Author Manuscript

NIH-PA Author Manuscript

NIH-PA Author Manuscript

NIH-PA Author Manuscript

Morris, 1987; Barnes et al., 1990; O'Reilly and McClelland, 1994; Rolls and Kesner, 2006). However, whether such differences arise from intrinsic properties of single cells or circuit effects is not well understood.

Previous single cell studies failed to find reliable regional differences (O'Keefe and Speakman, 1987; Bostock et al., 1991; Tanila, 1999; Knierim, 2002; Paz-Villagram et al., 2004; cf., Leutgeb and Leutgeb, 2007). In both regions, the majority of pyramidal cells give rise to similar firing fields controlled by distant and local cues. The firing pattern similarity can be explained by treating the CA3-CA1 system as a single computational unit, with one subset (CA1) embedded in the interconnected subset (CA3), in which CA1 neurons simply observe and integrate the output of CA3 neurons. Indeed, the computational results of the CA3 system can be conveyed to the neocortex only by way of the feed-forward CA1 circuit.

The recognition that the distinct layers of the entorhinal cortex convey different types of information to the CA3 and CA1 regions (Sargolini et al., 2006; Moser et al., 2008), led to more careful physiological investigations of these regions of the hippocampus. Indeed, several recent experiments spell out regional differences in firing patterns in response to various environmental manipulations (Lee et al., 2004a,b; Leutgeb et al., 2004, 2005; Vazdarjanova and Guzowski, 2004; Dragoi and Buzsaki, 2006; Lee and Knierim, 2007; Alvernhe et al., 2008; cf., Leutgeb and Leutgeb, 2007). Although the regional differences at the single neuron level may not be striking, it has been suggested that the cumulative effects of the contribution of many neurons amount to large and qualitatively different computations at the population level in the CA1 and CA3 regions (Leutgeb and Leutgeb, 2007).

Several previous works have examined the intrinsic, biophysical properties of both CA1 pyramidal cells (Spruston et al., 1995a; Magee and Johnston, 1997; Golding and Spruston, 1998; Kamondi et al., 1998; Golding et al., 2001; Golding et al., 2002; Gasparini et al., 2004; Jarsky et al., 2005; Losonczy et al., 2008) and CA3 pyramidal neurons (Traub et al., 1991; Jonas et al., 1993; Major et al., 1994; Turner et al., 1995; Debanne et al., 1998; McMahon and Barrionuevo, 2002; Kobayashi and Poo, 2004; Meeks and Mennerick, 2007; Pelkey and McBain, 2008). However, specific quantitative comparisons between the two cell types are rare (Spruston et al., 1995b; Poirazi and Mel, 2001; Spruston, 2008), and the impact of the intrinsic properties of neurons on their network behavior has remained largely unexplored. To gain insight into the physiological nature of the regional differences in the hippocampus, we have recorded from large sets of CA1 and CA3 pyramidal cells under various brain states and in different environments. The results showed reliable quantitative differences in state-dependent firing patterns, relationship to population oscillations, and place field properties between CA1 and CA3 neurons.

MATERIALS AND METHODS

Animal Surgery

Thirteen Long Evans rats (male, 250–400 g) were deeply anesthetized with isoflurane (1–1.5%). Details of surgery and recovery procedures have been described in detail (Csicsvari et al., 1999). In nine rats, high-density 32- or 64-site silicon probes were implanted in the dorsal hippocampus (Diba and Buzsaki, 2008; Mizuseki et al., 2009; Royer et al., 2010) and recorded from CA1 or CA3 pyramidal layers. Each shank had eight recording sites (160 μm each site, 1–3-Mμ impedance), and intershank distance was 200 μm. Recordings sites were staggered to provide a two-dimensional arrangement (20-μm vertical separation). In four rats, eight independently movable wire tetrodes aimed to record from the dorsal (one tetrode) and ventral part of the hippocampus (seven tetrodes; Royer et al., 2010). Only neurons recorded from the dorsal hippocampus are reported in this work. The silicon probes

NIH-PA Author Manuscript

NIH-PA Author Manuscript

NIH-PA Author Manuscript

and tetrodes were attached to micromanipulators and moved slowly to the target. Two stainless steel screws inserted above the cerebellum were used as indifferent and ground electrodes during recordings. At the end of the physiological recordings, a small anodal DC current (2–5 μA, 10 s) was applied to recording sites 1 or 2 days before sacrificing the animals. The rat was deeply anesthetized and perfused with 10% formalin solution. The position of the electrodes was confirmed histologically and reported previously in detail (Diba and Buzsaki, 2008; Mizuseki et al., 2009; Royer et al., 2010). All protocols were approved by the Institutional Animal Care and Use Committee of Rutgers University.

Behavioral Testing

After recovery from surgery (~ 1 wk), physiological signals during waking were recorded during six different tasks: (1) a task on the linear track (250 × 7 cm^2), (2) a task on the open field (180 × 180 cm^2or 200 × 100 cm^2), (3) a wheel running task, (4) an alternation task in the T-maze (100 × 120 cm^2) with wheel running delay were described previously (Mizuseki et al., 2009; Royer et al., 2010). (5) A radial maze in which the animals were trained to seek out water rewards at the end of each arm. Equal amounts of water (20 (μl) were added in all water wells regularly (~ every 30 s) so that those wells that had not been visited for longer periods of time accumulated more water (Royer et al., 2010). This approach ensured that the animals visited all arms with the same probability. (6) A zigzag maze, in which the animals learned to run back and forth between two water wells; 100 μl of water was delivered at each well (Royer et al., 2010). For tracking the position of the animals, two small light-emitting diodes, mounted above the head-stage, were recorded by a digital video camera.

Data Collection and Cell-Type Classification

Detailed information about the recording system and spike sorting has been described (Csicsvari et al., 1999; Diba and Buzsaki, 2008; Mizuseki et al., 2009; Royer et al., 2010). Briefly, signals were amplified (1,000×), bandpass-filtered (1–5 kHz) and acquired continuously at 20 kHz (DataMax system; RC Electronics) or 32 kHz (NeuraLynx, MT) at 16-bit resolution. After recording, the signals were down-sampled to 1,250 Hz for the local field potential (LFP) analysis. Positive polarity is up in all illustrations. Spike sorting was performed automatically, using KlustaKwik (http://klustakwik.sourceforge.net, Harris et al., 2000), followed by manual adjustment of the clusters (Klusters software package, http://klusters.sourceforge.net, Hazan et al., 2006). After spike sorting, we plotted the spike features of units as a function of time, and the units and sessions with signs of significant drift over the period of recording were discarded. Within the remaining data, only units with clear refractory periods and well-defined cluster boundaries were included in the analyses (Harris et al., 2000). Hippocampal principal cells and interneurons were separated based on their autocorrelograms, waveforms, short-term synaptic interactions, and mean firing rates (Skaggs et al., 1996; Csicsvari et al., 1999; Mizuseki et al., 2009). Firing properties of the interneurons are not discussed in this work.

Detection of Brain States

Theta periods during task performance (RUN), rapid eye movement (REM) sleep, and slow-wave sleep (SWS) were detected using the ratio of the power in theta band (5–11 Hz) to delta band (1–4 Hz) of LFP, followed by manual adjustment with the aid of visual inspection of whitened power spectra and the raw traces (Sirota et al., 2008; Mizuseki et al., 2009; Mizuseki et al., 2011). REM epochs were cross-validated with experimenter notes taken while observing theta activity on-line during sleep sessions to verify that the rat was sleeping (Mizuseki et al., 2011). Theta periods from all maze behaviors were lumped together as RUN.

NIH-PA Author Manuscript

NIH-PA Author Manuscript

NIH-PA Author Manuscript

Theta Phase Modulation

LFP was band-pass (5–11 Hz) filtered, yielding theta waves $y(t)$. Peaks of filtered waves were identified as the positive to negative zero crossings of the derivative $\frac{dy}{dt}$, and phase was linearly interpolated between the peaks. Peaks are at 0° and 360° and troughs at 180° throughout the paper. The mean direction and mean resultant length of the theta phases for a given neuron's spikes were taken as the preferred phase and modulation depth of that neuron, respectively. For the preferred phase and modulation depth, only neurons that were significantly modulated by the theta oscillations are shown. For the circular statistics of theta phase of single cells, only neurons with at least 50 spikes during theta epochs (RUN or REM) were used, and $P < 0.01$ (Rayleigh test) was used to define significantly theta-modulated neurons.

Spike Analysis

A burst index was defined as the ratio of spikes in bursts to all spikes. Inclusion of a spike in a burst event required a spike with an interspike interval (ISI) less than 6 ms occurred either before or after the spike. To compute the circular statistics of theta phase for single spikes and burst spikes, we first identified the single spikes and burst spikes of a neuron according to their ISIs. A spike in a burst whose length was 3 or more spikes was sorted into the burst spike category, whereas a spike associated with ISIs both before and after that spike larger than 20 ms was sorted into the single spike category. The preferred phase, modulation depth, and P value according to the Rayleigh test were calculated for each category of each neuron. If the number of spikes from a given cell in a given category was greater than 50, and the associated P value was less than 0.01, the cell was regarded as being significantly theta modulated within that category. For the autocorrelogram analysis, we removed the events at exact zero-time lag.

To quantify the theta modulation of cross-correlograms, we first normalized the cross-correlogram of all cell pairs so that the sum of probability during −400 to 400 ms is unity. The resultant cross-correlogram was band-pass filtered (5–12 Hz), and the amplitude of the filtered cross-correlogram was derived from the Hilbert transform of the filtered cross-correlogram. Mean of the amplitude of the filtered cross-correlogram (−400 to 400 ms) was taken as an index of theta modulation, and compared across states and cell groups.

Spatial Tuning of Spiking Activity

Radial and zigzag mazes—The position of the rat was projected along the axes of the arms of the maze. Each "linearized" arm of the maze was divided into 100 equal pixels (50 pixels for the zigzag maze's corner arms), and the number of spikes and occupancy times were calculated. The spike count and occupancy vectors obtained were smoothed by convolving them with a Gaussian function (5 pixels half-width). The firing field vector was represented as the ratio of "spike count vectors"/"occupancy vectors" (Royer et al., 2010).

Open field and linear track—For the linear track, the positions were projected onto the track axis. The position and spiking data were sorted into 5×5 cm^2 (open field) or 5 cm (linear track) pixels, generating the raw maps of spike number and occupancy. For the linear track, rate map, number of place fields, spatial information (Skaggs et al., 1993), spatial coherence (Muller and Kubie, 1989), stability (Markus et al., 1994), and phase precession (O'Keefe and Recce, 1993) were analyzed for each direction separately. A raw rate map was constructed by dividing a raw spike map by a raw occupancy map and then used to compute spatial coherence. The spatial coherence of each firing field was defined as the correlation between a list of firing rates in each pixel and a corresponding list of firing rates averaged

NIH-PA Author Manuscript

NIH-PA Author Manuscript

NIH-PA Author Manuscript

over the adjacent pixels of each pixel (eight adjacent pixels for the open fields, two adjacent pixels for the linear track, Muller and Kubie, 1989; Hafting et al., 2008).

Peak firing rate, number of place fields, stability, and spatial information were computed from the smoothed rate map. To construct smoothed rate maps for the open field, an adaptive smoothing algorithm was used (Skaggs et al., 1996; Henriksen et al., 2010). The firing rate at each pixel was estimated by expanding a circle around the pixel until

$$N_{\text{spikes}} > \frac{\alpha}{N_{\text{occ}}^2 r^2}$$

where N_{occ} is the occupancy time (second) in the circle, N_{spikes} is the number of spikes emitted in the circle, r is the radius of the circle in pixels, and a is a scaling parameter, set at 40,000. The firing rate at that pixel was then set to $\frac{N_{\text{spikes}}}{N_{\text{occ}}}$.

For the linear track, a Gaussian kernel (SD = 5 cm) was applied to both raw maps of spike and occupancy, and a smoothed rate map was constructed by dividing the smoothed spike map by the smoothed occupancy map. The starting segment (area at 0–25 cm) was excluded from the analysis to exclude the effect of turning and other behavioral variability.

A place field was defined as a continuous region, of at least 225 cm^2 (9 pixels) for the open field and 15 cm (3 pixels) for the linear track, where the firing rate was above 10% of the peak rate in the maze and the peak firing rate of the area was >2 Hz. Using a threshold of 20% of the peak rate gave similar results in most calculations (data not shown). Place map stability was defined by the pixel-by-pixel correlation coefficient between the firing rate maps of the first and second halves of the recording session. The spatial information content (Skaggs et al., 1993) was calculated according to the following formulae:

$$\text{Information per spike} = \sum_{i=1}^{N} p_i \frac{\lambda_i}{\lambda} \log_2 \frac{\lambda_i}{\lambda} \quad \text{Information per second} = \sum_{i=1}^{N} p_i \lambda_i \log_2 \frac{\lambda_i}{\lambda}$$

where $i = 1, \ldots, N$ represents pixel identification number, p_i is the probability of occupancy of pixel i, λ_i is the mean firing rate of pixel i, λ is the overall mean firing rate of the cell on the maze.

Calculation of indexes characterizing spatial correlation of spiking on the linear, zigzag, and radial mazes—A “directionality index” was calculated by computing the pixel-by-pixel correlation between firing rates during left (outbound) and right (inbound) journeys. A “symmetry index” was defined as the pixel-by-pixel correlation between firing rates during left (outbound) and reversed right (inbound) journeys (Royer et al., 2010). A “repetition index” was defined as the pixel-by-pixel firing rate correlation between the equivalent corridors in the zigzag maze when the animal was running in the same direction. A “similarity index” was defined as the pixel-by-pixel firing rate correlation between the same (same) or different (different) type of arms of the radial maze when the animal was running in the same direction (outbound or inbound).

Phase Precession Analysis

The strength of phase precession on the linear track was quantified by calculating theta phase–position correlation as described previously (Hafting et al., 2008; Mizuseki et al., 2009). Briefly, the place field was identified using >2 Hz peak firing rate and >0.7 spatial

NIH-PA Author Manuscript

NIH-PA Author Manuscript

NIH-PA Author Manuscript

coherence as criteria. Place fields with fewer than 50 spikes and fields that included the turning position of the track were discarded (Hafting et al., 2008; Mizuseki et al., 2009). The theta phases of spikes were displayed as a function of the rat's position, and the theta phase–position correlation was determined by parametrically rotating the phase by the position matrix for each place field. Phase rows were shifted by 1° steps from 0° to 360°. For each rotation, a linear regression curve was fitted. The correlation between theta phase and the rat's position (the distance from the start of the place field on the linear track) at the phase rotation that gave the regression line with the largest explained variance R^2 was used as the phase-position correlation. In some cases, this objective and automatic method gives a spurious positive correlation value even when visual inspection suggest negative correlation (see also Hafting et al., 2008). The degree of phase advancement was quantified by computing mean circular phase for each 10% segment of the firing field (Huxter et al., 2003; Hafting et al., 2008; Mizuseki et al., 2009). Data analysis was carried out by custom-written MATLAB-based software.

RESULTS

LFP and unit firing were recorded from the septal third of hippocampal CA1 and CA3 pyramidal layers in 13 rats (3,670 CA1 pyramidal cells from 13 rats and 2,203 CA3 pyramidal cells from six of the rats). In three animals, recordings were made simultaneously in CA1 and in multiple layers of the medial entorhinal cortex and in another three rats units were recorded simultaneously from CA1 and CA3 neurons. Histological localization of the electrodes, criteria for clustering single units and separation of pyramidal cells and interneurons in these animals have been described in detail previously (Diba and Buzsaki, 2008; Mizuseki et al., 2009; Royer et al., 2010). Recordings were carried out while the animal either ran on an open field (200 × 100 cm^2, 180 × 180 cm^2), a linear track (250 cm long), a radial arm maze with seven 75-cm arms or a zigzag maze (100 × 200 cm^2), or performed a wheel running task and an alternation task in the T-maze (Mizuseki et al., 2009; Royer et al., 2010). Theta periods from all maze behaviors were lumped together as RUN. Recordings were also carried out during sleep, including several epochs of REM sleep and SWS in the animal's home cage, typically both before and after the behavioral sessions.

Firing Patterns of CA1 and CA3 Pyramidal Cells

The overall firing rates of CA1 neurons were significantly higher than those of CA3 cells in each brain state (RUN, REM, and SWS; $P < 0.0001$, $P < 0.0001$, and $P < 0.0001$, t-test). However, the different brain states exerted quantitatively different effects on the two cell groups, as reflected by the significant cell group × brain state interaction (Fig. 1A; $P_{state} < 0.0001$, $F_{2,\ 12519} = 46.4$, $P_{GROUP \times STATE} < 0.02$, $F_{2,\ 12519} = 4.17$, ANOVA). The highest mean firing rates were observed during RUN (CA1 = 0.88 ± 1.23 Hz; CA3 = 0.50 ± 0.78 Hz), followed by SWS (CA1 = 0.72 ± 0.78 Hz; CA3 =0.42 ± 0.44 Hz) and REM (CA1 = 0.67 ± 1.00 Hz; CA3 = 0.24 ± 0.38 Hz), in both regions. While the mean rates during REM and SWS were only slightly different in CA1, mean discharge rate during REM sleep was much lower than during SWS in CA3 pyramidal cells (Fig. 1; Montgomery et al., 2008).

To examine how states affect individual neurons, the distribution of rates across pairs of states was also calculated (Fig. 1C). Indeed, the magnitudes of rate shift were different when the discharge rates of the same neurons were compared across states than when the means of the populations between states were compared (compare Figs. 1A,B). The state-dependent rate shift of individual neurons was significantly different between CA1 and CA3 pyramidal cells in all comparisons (Fig. 1D; $P < 0.001$, $P < 0.0001$, and $P < 0.0001$, rank sum test), with the largest rate shift present between SWS and REM sleep of CA3 pyramidal cells.

NIH-PA Author Manuscript

NIH-PA Author Manuscript

NIH-PA Author Manuscript

The temporal dynamic of firing patterns of single neurons was examined by spike autocorrelograms, interspike-interval histograms and the burst index of neurons. Each of these measures showed that short ISIs (i.e., bursts; Ranck, 1973) were significantly more prevalent among CA3 neurons (Figs. 2A – C). Analysis of both autocorrelograms and ISI histograms (Figs. 2A,B) revealed large peaks between 2 and 6 ms, corresponding to intraburst ISIs. The peak of interspike-interval histograms occurred at significantly shorter ISIs in CA3 than in CA1 neurons (CA1 = 5.04 ± 1.00; CA3 = 4.29 ± 1.12; mean ± SD, $P <$ 0.0001, *t*-test, using all the data regardless of brain states). At longer interpike intervals, the histogram count continued to decrease exponentially, an indication that a burst is a renewal process rather than an all-or-none event (Harris et al., 2001). Therefore, for further analysis, we used a traditionally adopted criterion for bursts and defined a “complex spike burst” as a series of two or more spikes with <6 ms intervals (Ranck, 1973). The spike-burst index was defined as the fraction of spikes with <6 ms ISIs (Harris et al., 2001). The burst index was highest during SWS and lowest during RUN in both neuron types but CA3 neurons were almost twice as likely to fire at ISIs <6 ms (Fig. 2C). “Burst length” was defined as the number of spikes emitted at <6 ms intervals. The number of spikes in a burst varied within bursts of a single neuron, as well as between neurons. The probability of seeing n spikes in a burst decreased supraexponentially with n, as reflected by the deviation from the linear fit of burst length probability on a logarithmic scale (Fig. 2D; Metzner et al., 1998; Harris et al., 2001). This “spike renewal” process was stronger for CA3 than CA1, that is, CA3 pyramidal cells had a higher probability of long bursts. The impact of state on region differences was significantly larger for longer bursts, especially for bursts with five or more spikes (Fig. 2F; $P_{\text{region}} < 0.0001$, $F_{1,11803} = 208.8$; $P_{\text{state}\times\text{region}} < 0.0001$, $F_{2,11803} = 85.9$).

The probability of burst occurrence and burst length depended on the duration of the silent (nonspiking) period before the burst in a complex manner. To express these features more explicitly, burst probability (two or more spikes at <6 ms) was plotted as a function of previous ISI in Figure 2E. The probability of burst for CA1 pyramidal cells increased with the silent period and reached a maximum at ~ 100 ms, after which it decreased again (Fig. 2E; Harris et al., 2001). This dynamics could reflect intrinsic features of CA1 pyramidal cells because a peak at this interval was prominent not only in RUN and REM states but also during SWS. In contrast, CA3 pyramidal neurons did not have a peak at 100 ms during SWS, only during RUN and REM. Similar results were obtained using <8 ms and <10 ms interspike interval burst definition (not shown). The relationship between firing rate and burstiness was also different between CA1 and CA3 pyramidal cells (Fig. 2G). In CA1 pyramidal neurons, there was a positive relationship between the bursting index and the firing rate of individual neurons. In contrast, an inverted-U relationship was present in CA3 neurons, where the highest burst rate was correlated with an intermediate discharge frequency. Similar positive and inverted-U relationships were obtained when neurons were examined in RUN, REM, and SWS sessions separately (data not shown).

Examination of the autocorrelograms of single spikes and bursts separately showed further evidence for state-dependent differences in firing patterns of CA1 and CA3 neurons. In this analysis, bursts (three or more spikes at <6 ms) were treated as single events. Bursts showed a more prominent oscillatory pattern in the theta band than single spikes during both REM and RUN (Fig. 3A). Further, bursts of CA1 pyramidal cells showed significantly stronger theta period modulation than CA3 pyramidal cells, measured by the ratio of events in the interval [−65 and 65] ms to events in the interval [−400 and 400] ms (during RUN; CA1 = 0.064, CA3 = 0.132, $P < 0.0001$; during REM; CA1 = 0.074, CA3 = 0.201, $P < 0.0001$, median, rank sum test). During SWS, the autocorrelograms of single spikes of CA1 and CA3 pyramidal cells were similar and had a high central peak (Fig. 3A). In contrast, burst autocorrelograms showed a striking difference between CA1 and CA3. CA1 bursts showed a maximum probability at ~ 100 ms, whereas CA3 burst probability was elevated at short ISIs

NIH-PA Author Manuscript

NIH-PA Author Manuscript

NIH-PA Author Manuscript

(0–50 ms). The state dependence of firing patterns is further illustrated by comparing the length of silent period occurring before bursts of various lengths (Fig. 3B). In CA1, the length of bursts and the length of preceding silent periods were correlated positively in all states. In contrast, the relationship between the length of bursts and the length of preceding silent periods in CA3 cells was state dependent, as the length of preceding silent periods was relatively independent of burst length during REM, varied positively with burst length during SWS and negatively during RUN (Fig. 3B). Overall, these findings show that whereas intrinsic biophysical properties of CA1 and CA3 pyramidal cells are important for determining firing properties, these properties vary distinctly in CA1 and CA3 neurons in different network states.

Distinct Environments Differentially Affect CA1 and CA3 Pyramidal Neurons

Open field—As place cell activity is most often assessed in two-dimensional environments (O'Keefe and Nadel, 1978; O'Keefe and Burgess, 1996), we first examined the discharge behavior of pyramidal cells in the open field (Fig. 4). Place cells were defined by two methods. First, a place field was defined as a contiguous set of pixels of at least 225 cm^2 where the firing rate was above 10% of the peak rate in the field and the peak firing rate was >2 Hz (additional calculations were also made for 0.5, 1, and 4 Hz peak firing rates and 20% peak rate criteria, and the results were similar). The second method used the same criteria, plus an additional criterion of spatial coherence >0.7 (See Methods). By peak rate criterion alone, significantly larger fraction of CA1 than CA3 neurons had definable place fields (Fig. 5A; CA1 = 74.7%; CA3 = 59.6%; $P < 0.0001$; χ^2 test). Spatial coherence for fields identified by rate criterion alone was slightly but significantly lower for CA1 than CA3 neurons (Fig. 5B, CA1 = 0.58, CA3 = 0.62, $P < 0.01$; rank sum test). When defined by both rate and spatial coherence, the fraction of neurons with place fields in the open maze was comparable between CA1 and CA3 neurons (CA1 = 37.3%; CA3 = 37.9%; $P > 0.5$). The majority, and similar fraction, of both CA1 and CA3 neurons had single place fields (Fig. 5C; >2 Hz peak, 10% peak firing rate in the maze and >0.7 spatial coherence criteria). The mean place field size was significantly larger for CA1 (1,775 cm^2, median) than CA3 neurons (1,275 cm^2; $P < 0.0001$, rank sum test; Fig. 5D). Similarly, spatial coverage, defined by the fraction of pixels with firing rates >20% of the peak firing rate of the neuron, was also significantly larger for CA1 cells (Fig. 5E; CA1 = 9.2%, CA3 = 7.2%, $P < 0.05$). In line with the smaller place field size in CA3 pyramidal cells, the spatial information content of spikes (Skaggs et al., 1993) was significantly larger in CA3 (1.77 bits per spike) than in CA1 (1.31 bits per spike; median, $P < 0.00001$, rank sum test; Fig. 5F). The peak firing rate (CA1 = 12.4 Hz, CA3 = 13.5 Hz, $P > 0.05$) and within-field firing rate were not significantly different between cell groups (CA1 = 4.60 Hz, CA3 = 5.12 Hz; $P > 0.05$; Fig. 5G). We also examined place field stability by calculating the correlation (r) of firing rates in each pixel between the first and second halves of the recording sessions. CA1 pyramidal neurons were significantly less stable compared to CA3 cells (Fig. 5H; CA1 = 0.82, CA3 = 0.85, $P < 0.0001$). The information rate, expressed in bit per second (Skaggs et al., 1993), was not different across the groups (CA1 = 1.33; CA3 = 1.24; $P > 0.1$). The discrepancy between the results of information per spike and information per second can be explained by the higher mean firing rate during the task in CA1 than in the CA3 pyramidal cells (Fig. 1A, Leutgeb et al., 2004). In summary, CA3 pyramidal cells were more compact, more stable and carried more spatial information per spike than their CA1 peers.

Linear maze—Place fields in the linear maze were identified by the contiguous pixels where the neuron's firing rate exceeded 10% of the peak firing rate, with peak rates >2 Hz and spatial coherence >0.7 (Hafting et al., 2008; additional calculations were also made for 0.5, 1, and 4 Hz peak firing rates and 20% tail criteria with similar results). Both CA1 and CA3 pyramidal cells relatively evenly covered the entire length of the linear track (Fig. 6). A

NIH-PA Author Manuscript

NIH-PA Author Manuscript

NIH-PA Author Manuscript

major difference between the two groups was the fraction of place cells. By both peak rate criterion alone (Fig. 7A; CA1 = 64.2%; CA3 = 31.0%; $P < 0.0001$; chi-square test) and by combined peak and spatial coherence criteria (CA1 = 48.0%; CA3 = 16.8%; $P < 0.0001$), a robustly larger fraction of CA1 than CA3 pyramidal cells had definable place fields. Spatial coherence for fields identified by the rate criterion was comparable between the two groups ($P > 0.05$; rank sum test). When defined by both rate and spatial coherence, the number of place fields was comparable between CA1 and CA3 neurons, and similar fraction of CA1 and CA3 neurons had single place fields (Fig. 7B; >2 Hz peak, 10% tails, >0.7 spatial coherence criteria). Both neuron types were strongly directional (Fig. 6 and Fig. 7C; McNaughton et al., 1983), i.e., their positional representations differed significantly during left and right journeys but no difference was found between the two groups (directionality index, CA1 = −0.01, CA3 = −0.08, $P > 0.1$, rank sum test). A subset of neurons in both regions showed a mirror image of their firing patterns during the left and right journeys. A symmetry index was calculated by computing the pixel-by-pixel correlation between firing patterns of neurons during left and reversed right journeys (Royer et al., 2010). The symmetry index was significantly different between the two neuronal groups (Fig. 7D, CA1 = −0.15, CA3 = − 0.08, $P < 0.001$). The mean place field size was significantly larger for CA1 (75 cm) than in CA3 (50 cm; $P < 0.0001$; Fig. 7E). The information content of spikes was significantly smaller in CA1 (0.83 bits per spike) versus CA3 pyramidal cells (1.57 bits per spike; $P < 0.0001$; Fig. 7F), and place field stability of CA1 pyramidal neurons was significantly less compared to CA3 cells (CA1 = 0.90, CA3 = 0.95, $P < 0.0001$, Fig. 7G). Information rate (bits per second) was similar between the groups (CA1 = 2.69, CA3 = 2.76, $P > 0.2$). Neither the infield firing rate (7.5 Hz; Fig. 7H) nor peak firing rate (14.5 Hz) of CA1 pyramidal cells was significantly different from CA3 (in-field = 7.1 Hz; peak = 12.4 Hz) pyramidal cells. In summary, fewer CA3 pyramidal cells form place fields on the linear track but their fields are more compact, more stable, and carry more spatial information per spike than CA1 neurons.

Radial arm maze: The majority of CA1 and CA3 pyramidal cells had only one or two place fields in the radial maze (Fig. 8; Olton et al., 1979; McNaughton et al., 1983), and multiple active arms were more prevalent in CA3 than in CA1 cells (Fig. 9B; $P < 0.01$; rank sum test). In contrast to the linear track, where most neurons were silent in the “nonpreferred direction,” many neurons were active in both directions on the same arm in the radial maze (compare Fig. 9A, arrows pointing to the “ghost” diagonal pattern, and Fig. 6). Many CA1 and CA3 neurons fired at similar positions during reward-bound and center-bound travels, as measured by the high positive directionality index values (CA1 = 0.63, CA3 = 0.62, $P > 0.5$, Fig. 9D) and negative symmetry index values (CA1 = −0.40, CA3 = − 0.33, $P < 0.01$, Fig. 9E). Two different arms were equally similarly (or dissimilarly) represented by CA1 and CA3 pyramidal cells regardless of the type of arms, as quantified by the similarity index, i.e., the pixel-by-pixel correlation of firing rates in identical arms (CA1 = −0.04, CA3 = −0.03, $P > 0.1$; Fig. 9F; Alvernhe et al., 2008; Royer et al., 2010) and different arms (CA1 = 0.03, CA3 = 0.01, $P > 0.1$, Fig. 9G). As on the linear track, the median place field size of CA1 neurons was significantly larger (38.3 cm) than that of CA3 cells (33.8 cm; $P < 0.01$, Fig. 9C). In summary, in contrast to the linear maze, CA3 pyramidal cells had more place fields than CA1 cells, although the CA3 place fields were smaller than those of CA1 pyramidal cells. Both CA1 and CA3 neurons were much less directional in the radial arm mazed (i.e., they tended to fire in both directions in the same arm) than on the linear track.

Zigzag maze—In the zigzag maze, the rat travels through two geometrically identical corridor configurations before reaching the reward. Both distant cues (O’Keefe and Nadel, 1978) and the travel path (McNaughton et al., 1996) can affect hippocampal firing patterns in identical corridor segments (Fig. 10; Derdikman et al., 2009). The majority of CA1

NIH-PA Author Manuscript

NIH-PA Author Manuscript

NIH-PA Author Manuscript

pyramidal neurons fired repeatedly in geometrically identical corridors of the zigzag maze (note double diagonal bands of activity in Fig. 11A), reminiscent of the "path equivalence" firing patterns of entorhinal cortical neurons (Frank et al., 2000; Derdikman et al., 2009) and CA1 pyramidal cells (Nitz, 2011). The correlations between the firing patterns in the two corridors were strongly skewed towards one in CA1 pyramidal cells but less so in CA3 cells (Fig. 11C; repetition index, $r = 0.78$ for CA1; $r = 0.32$ for CA3; $P < 0.0001$, rank sum test). Directionality of firing was similar to that observed on the linear track (Fig. 11D; $r = 0.23$ for CA1; $r = 0.11$, CA3; $P < 0.01$). Pixel-by-pixel correlation of firing rates between left-bound and reversed right-bound travels (i.e., the "symmetry index") were low for both groups (Fig. 11E). However, in a subset of CA1 neurons, the symmetry index was close to 1, and the symmetric index was significantly more positive for CA1 than CA3 cells (Fig. 11F; $r = 0.02$ for CA1; $r = -0.03$ for CA3; $P < 0.01$; rank sum test). The place field size was significantly larger in CA1 than in CA3 cells (Fig. 11B; CA1 = 48 cm, CA3 = 34 cm, respectively; $P < 0.01$ rank sum test). In summary, CA3 neurons in the zigzag maze had smaller place fields, firing typically only in one of the corridors. In contrast, the majority of CA1 neurons fired repeatedly in the two corridors, and a subset of CA1 cells discharged in a mirror-symmetric manner during left and right journeys. The findings suggest that neither distant room cues nor local apparatus cues alone can fully account for the firing patterns of all hippocampal pyramidal cells.

Spike Modulation of CA1 and CA3 Neurons by Theta Oscillations

Neurons in all regions of the hippocampus are strongly modulated (i.e., phase-locked) to theta oscillations (Buzsaki et al., 1983). CA3 pyramidal cells were significantly more strongly phase-locked to theta than CA1 cells (Figs. 12A–C; "mean resultant length," Mizuseki et al., 2009). A large part of this difference stemmed from the different rate-phase sensitivity of the two groups (Mizuseki et al., 2009). Whereas the shift between the phase preference of single spikes (>20 ms ISIs) and bursts (three or more spikes at <6 ms intervals) was relatively small for CA3 neurons (<90°), phase preference of bursts was broad in CA1 pyramidal cells, and most bursts occurred at the peak of the theta wave, as opposed to the trough for single spikes. Bursts, in both regions, and especially in the CA1 region, were more strongly phase-modulated by theta oscillations than single spikes (Fig. 12C; $P < 0.0001$).

The narrower range of theta phase preference of CA3 pyramidal cells was also evident from the significantly more strongly theta-modulated cross-correlograms of CA3 pairs compared to CA1 neuron pairs during both RUN and REM (Fig. 13). This was true for both single spikes (RUN, $P < 0.0001$; REM, $P < 0.0001$, rank sum test) and bursts (2 or more spikes at < 6 ms; RUN, $P < 0.0001$; REM, $P < 0.0001$, Fig. 13). During SWS, cross-correlograms of single spikes of CA1 neurons had a significantly larger central peak compared to CA3 (Fig. 13A; $P < 0.0001$, −45 to 45 ms), whereas the cross-correlograms of bursts of CA3 pyramidal neurons showed a larger peak than those of CA1 bursts (Fig. 13C; $P < 0.0001$). Thus, the direction of the synchrony of the CA1 and CA3 pyramidal cell populations depend on both firing patterns of the neurons and the state of the hippocampal network.

The spike autocorrelograms of both CA1 and CA3 pyramidal cells showed a peak at theta frequency (Fig. 14A). Closer examination of the peaks revealed that the oscillatory intervals between spikes of CA3 pyramidal cells were significantly shorter than those of CA1 cells (Fig. 14A; $P < 0.0001$) and shorter than the intervals between LFP theta troughs (i.e., the period of the theta cycle; black lines in Fig. 14A; $P < 0.0001$, $P < 0.0001$, respectively). This was also true when only spikes during bursts (two spikes or more at < 6 ms) were used for the construction of the autocorrelogram (Fig. 14A, $P < 0.001$, $P < 0.0001$, $P < 0.0001$). Such frequency differences between two oscillators (neuron vs. LFP) generate phase interference. Indeed, hippocampal place cells have been shown to discharge at progressively earlier

NIH-PA Author Manuscript

NIH-PA Author Manuscript

NIH-PA Author Manuscript

phases of the theta cycle as the rat moves through the firing field of the neuron (Fig. 14B; O'Keefe and Recce, 1993; Skaggs et al., 1996). It has been postulated that the size of place field depends on the intrinsic oscillation frequency of a neuron (Maurer et al., 2005). The shorter intervals between spike trains of CA3 pyramidal neurons (i.e., their higher oscillation frequencies) are congruent with the smaller place fields of CA3, relative to CA1 neurons.

Phase precession (O'Keefe and Recce, 1993) on the linear track was quantified for each firing field with >2 Hz peak firing rate and >0.7 spatial coherence (Hafting et al., 2008). CA1 neurons showed a slightly sigmoid phase shift with position, and the phase-shift exceeded 200° within the place field (Figs. 14B – D). CA3 neurons showed a comparable shift in the rising part of the field, whereas little further phase shift occurred in the falling part of the field (Figs. 14B,C). To examine whether this difference emanated from the different shape of theta waves in the CA1 and CA3 pyramidal layer (Montgomery et al., 2008), we recalculated the mean slopes using the LFP from Layer 3 of the entorhinal cortex (Mizuseki et al., 2009). The difference of the slope between the CA1 and CA3 in the second half of the place field remained similar (Fig. 14C, right). The "phase span" within the field was determined by subtracting the preferred phase of spiking at the end and beginning of the field. The beginning and the end of the field were determined as positions where the firing rate rose 10% above and fell below 10% of the peak rate, respectively. CA1 pyramidal neurons had a significantly larger phase span (230°, median) compared to CA3 neurons (154°; $P < 0.0001$, rank sum test; Fig. 14D), reminiscent of the more restricted phase precession of neurons in the dentate gyrus (Skagg et al., 1996). The difference in phase precession dynamic between CA3 and CA1 cannot be explained by firing rate, because neither the in-field firing rate (7.5 Hz; Fig. 7H) nor peak firing rate (14.5 Hz) of CA1 pyramidal cells was significantly different from CA3 (in-field = 7.1 Hz; peak = 12.4 Hz) pyramidal cells ($P_s > 0.05$). The differences of phase precession features between CA1 and CA3 pyramidal cells are also illustrated by the distribution of the phase versus position correlation. The spike phases of CA1 place cells were significantly more strongly (and negatively) correlated with position within the field than CA3 neurons (Fig. 14E; $P < 0.0001$), due mainly to the relatively poor phase-location relationship of CA3 neurons in the outbound part of the place field. Bursts of CA1 pyramidal cells (three spikes or more at < 6 ms intervals) showed the strongest theta phase–position relationship, whereas single spikes of CA3 pyramidal neurons were less reliable, with many CA3 neurons showing phase retardation (Fig. 14E).

Place fields on the track were rarely symmetric (Skaggs et al., 1996; Mehta et al., 1997). Instead, the place field of CA1 pyramidal neurons was skewed, on average, toward the outbound part of the field, whereas CA3 cells were skewed to the inbound part (Fig. 14F, median skewness, −0.21 for CA1, 0.07 for CA3, $P < 0.0001$, rank sum test). The field asymmetry was less pronounced but also present when only single spikes were analyzed (median skewness, −0.17 for CA1, 0.02 for CA3, $P < 0.0001$). For spike bursts (three spikes or more at <6 ms intervals) the field skewness was especially robust because most bursts of CA3 neurons occurred in the inbound part whereas more bursts were present in the outbound part of the place field of CA1 neurons (Fig. 14F, median skewness, −0.23 for CA1, 0.15 for CA3, $P < 0.002$).

DISCUSSION

Hippocampal CA1 and CA3 pyramidal cells differed in firing rates, spike bursts, and other aspects of spike dynamics in a brain state-dependent manner. Place fields were less frequently formed by CA3 pyramidal cells; yet, place fields of CA3 neurons were more compact, more stable and carried more spatial information per spike than those of CA1 pyramidal cells, whereas other features depended on the testing environment. CA3 neurons

NIH-PA Author Manuscript

NIH-PA Author Manuscript

NIH-PA Author Manuscript

were more strongly locked to the theta cycle but showed less pronounced phase precession and weaker position versus spike phase relationship than CA1 cells.

Spike Dynamics and Theta Phase Relationship of CA1 and CA3 Pyramidal Cells

Although the overall firing rates of CA1 neurons were significantly higher than those of CA3 cells, the magnitude of the difference between the two groups was largest in REM sleep (Montgomery et al., 2008). Most of CA3 pyramidal cells fired at lower rate during REM sleep than during slow wave sleep.

Bursts (i.e., spikes with <6 ms intervals; Ranck, 1973) were most prevalent during SWS and least during RUN. Both burst occurrence and burst length were higher in CA3 than CA1 neurons. Several models of spike burst generation propose that a burst is facilitated by activation of dendritic Ca^{2+} currents, which are enhanced by somadendritic back-propagation of the action potential (Wong and Prince, 1981; Pinsky and Rinzel, 1994; Traub et al., 1994; Andreasen and Lambert, 1995; Larkum et al., 1999; Magee and Carruth, 1999; Takahashi and magcc, 2009). In CA1 pyramidal cells, the main regulator of back-propagation is the availability of fast inactivating Na+ channels, which may take several hundreds of milliseconds to recover after each spike (Spruston et al., 1995a; Jung et al., 1997; Mickus et al., 1999). This hypothesis is supported by our observation of a positive relationship between the burst length and the length of the preceding nonspiking period in CA1 pyramidal cells. CA3 neurons, however, may follow different rules. The burst length in CA3 pyramidal cells was correlated positively with the silent period in SWS as in CA1 but negatively in RUN, and burst length was independent from the silent period in REM. An alternative explanation for the state dependence of burst propensity involves the neuromodulation of the persistent Na^+ current (I_{Nap}, Azouz et al., 1996; Su et al., 2001) or muscarine-sensitive K^+ current (I_M, Yue and Yaari, 2004), both of which regulate after depolarizations and both of which are strongly affected by subcortical neurotrans-mitters. The burst propensity at theta frequency in both regions, especially in CA1, might reflect resonant properties of these neurons (Leung and Yu, 1998; Pike et al., 2000; Hu et al., 2002; Rotstein et al., 2005; Hu et al., 2009; Leung, 2011).

Differences in Behavioral Correlates of CA3 and CA1 Pyramidal Cells

Our findings indicate that differences in place representations between the CA1 and CA3 regions depend on both the testing environment and methods of comparison (Muller and Kubie, 1987). Whereas approximately half of the CA1 pyramidal cells displayed well-defined place fields on the linear track by the combined rate (>2 Hz) and spatial coherence (>0.7) criteria (Hafting et al., 2008), only 20% of CA3 pyramidal cells did. The fraction of place cells on the open maze was considerably smaller for CA3 than CA1 neurons, consistent with previous observations (Leutgeb et al., 2004). Albeit a smaller fraction, CA3 place cells had more compact and more stable fields and carried more spatial information per spike than their CA1 peers, as indicated by earlier studies (Barnes et al., 1990; Park et al., 2011).

“Context” is often used as a classifier of firing fields (Leutgeb and Leutgeb, 2007). When rats are tested in different rooms (i.e., in different contexts), place cells “remap” (Muller and Kubie, 1987), and CA3 cells do so more coherently as a population than their CA1 peers (Leutgeb et al., 2004; Lee et al., 2004a,b; Leutgeb et al., 2005; Guzowski et al., 2004). Firing patterns of CA3 pyramidal cells reliably distinguish between two interconnected but physically identical boxes (Tanila, 1999), whereas CA1 pyramidal cells were much less able to do so (Skaggs and McNaughton, 1998; Paz-Villagrán et al., 2004). In a related experiment, removal of a wall section of the testing maze allowed the rat a shortcut. Place

NIH-PA Author Manuscript

NIH-PA Author Manuscript

NIH-PA Author Manuscript

fields of CA3 neurons far away from the shortcut route were more strongly affected than those of CA1 (Alverne et al., 2008).

In our experiments, CA3 neurons had smaller place fields in all environments than CA1 neurons. Other features of their patterns, however, showed a strong dependence of the testing conditions or context. The radial arm maze can be conceived of as a long single path where the continuous run is interrupted by turns in the center platform and rewards at the ends of the arms. Despite the multiple turns and rewards, most neurons formed a single place field on a single arm, irrespective of whether the arms were physically identical or dissimilar (by walls, color, and texture). The multiple corridors of the zigzag maze may also be conceptualized as a long single track. As in the radial maze, the rat had to turn several times (six times left, six times right). However, identical corridors of the zigzag maze were treated as identical by the majority of CA1 but not CA3 cells.

Derdikman and coworkers (2009) also observed repeating firing patterns (path equivalence patterns, Frank et al., 2000) in a zigzag maze with multiple identical compartments. They attributed the repeating patterns of entorhinal grids cell to the reset of a hypothetical “path integrator” (Hafting et al., 2005) by the turning movement of the rat and assumed that the hippocampal map mirrors the representation shifts of the entorhinal grid system. The turn-reset hypothesis of grid cells may not adequately explain our observations. First, the turn-reset hypothesis predicts stronger correlations of firing patterns between the repeating compartments in CA3 than in CA1 neurons, as grid cells constitute the majority of cells in Layer 2 but only a minority in Layer 3 of the entorhinal cortex (Sargolini et al., 2006). However, we found the opposite relationship. Second, path equivalence cells are abundant in deep layers of the entorhinal cortex (Frank et al., 2000) where grid cells are rare (Sargolini et al., 2006). Third, the rat performed sharp turns also in the radial arm maze, however, repeating patterns in the different arms were exceptionally rare. Instead of the turns, input from the head direction system (Taube, 2007) might explain the observed difference between zigzag maze and radial maze, as head direction is identical at the repeating corners on the zigzag maze but different at the turning points on the radial maze. The mirror symmetric, goal-directed firing of neurons (Hok et al., 2007; Royer et al., 2010) in the ziggag maze, more prevalent in CA1, is also difficult to explain by grid cell activity but they may be related to “border cells” of the entorhinal cortex (Solstad et al., 2008).

The distinct temporal firing patterns in the CA3 and CA1 regions questions the hypothesis that the hippocampal place cells simply integrate the entorhinal grid information (Mizuseki et al., 2009). It is unlikely that the spikes of CA1 pyramidal cells were exclusively timed by their entorhinal Layer 3 inputs, as most Layer 3 pyramidal cells show no or very little phase precession (Hafting et al., 2008; Mizuseki et al., 2009). Multisynaptic inheritance of grid cell activity by way of the dentate-CA3-CA1 route is also unlikely, as spike phase versus position relationships in the CA3 and CA1 regions were quite different. Furthermore, both single spikes and bursts of CA3 occurred at similar theta phases, whereas CA1 single spikes and bursts occurred out of phase.

The large differences in representation between the CA1 and CA3 regions raise the important question of why it is advantageous for the CA3 network to generate a higher resolution map when the readout of this information by the neocortex can occur only through the firing patterns of CA1 neurons. One potential answer is that CA1 pyramidal cells integrate the high granularity of CA3 inputs. Albeit this process comes with some loss of information content at a single cell level, the CA1 population can form a rich combinatorial route matrix of the CA3-represented places. The larger fraction of well-defined place cells in the CA1 region is in support of this speculation. A related argument is that the more compact and more strongly anchored CA3 place fields do not reflect local

NIH-PA Author Manuscript

NIH-PA Author Manuscript

NIH-PA Author Manuscript

sensory cues or better sensorial “triangulation” of the rat’s position relative to distant reference landmarks (O’Keefe and Nadel, 1978) but, instead, an internally generated assembly sequence of a travel route plan (Wood et al., 2000; Frank et al., 2000; Fenbinteanu and Shapiro, 2003; Wills et al., 2005; Ainge et al., 2007; Pastalkova et al., 2008; Gill et al., 2010), the details of which are important only at alternative routes, which can be read out by the CA1 system. Furthermore, the CA1 readout of the CA3 information may have a different format in different states. During off-line (non-theta) states of the hippocampus, hippocampal sharp wave-ripples in the CA1 region (Buzsaki et al., 1983; Buzsaki et al., 1992) may faithfully read out a different topographic content of the CA3 relationships. In support of this hypothesis, it has been shown that even nearby single CA3 pyramidal cells can be associated with topographically separated CA1 ripples (Csicsvari et al., 2000).

Further Subdivisions of the Cornu Ammonis Regions

Overall, the present findings show robust differences between CA1 and CA3 pyramidal neurons in terms of multiple single cell and circuit parameters and behavioral correlations. For simplicity, our comparisons have tacitly assumed that neurons in these respective regions are homogeneous. However, numerous recent experiments have found reliable differences in different subregions (Henriksen et al., 2010) and sublayers (Mizuseki et al., 2011) of CA1 pyramidal cells. Striking differences in plasticity have been revealed between the CA2 and CA3 regions (Chevaleyre and Siegelbaum, 2010; Jones and McHugh, 2011). Given the fundamental wiring differences between the CA3 subregions (Ishizuka et al., 1990; Li et al., 1994; Amaral and Lavenex, 2007), it is expected that gradual or discrete changes are also present across these subregions. Finally, robustly different features in single cell properties and behavioral correlates of pyramidal cells are present between the dorsal and ventral segments of the hippocampus (Maurer et al., 2005; Kjelstrup et al., 2008; Royer et al., 2010). Systematic documentation of the firing patterns and behavioral correlations in the different subregions, layers, and segments of the hippocampal formation are needed for a full appreciation of the complexity of circuit dynamics and cellular interactions in the hippocampus.

Acknowledgments

The authors thank M. Belluscio, S. Fujisawa, J. Long, and A. Peyrache for comments on the manuscript.

Grant sponsor: National Institute of Health; Grant number: NS34994 and MH54671; Grant sponsors: Grants, the Human Frontier Science Program, Howard Hughes Medical Institute, James S. McDonnell Foundation, the Uehara Memorial Foundation, and the Japan Society of Promotion for Sciences.

REFERENCES

Ainge JA, van der Meer MA, Langston RF, Wood ER. Exploring the role of context-dependent hippocampal activity in spatial alternation behavior. Hippocampus. 2007; 17:988–1002. [PubMed: 17554771]

Alvernhe A, Van CT, Save E, Poucet B. Different CA1 and CA3 representations of novel routes in a shortcut situation. J Neurosci. 2008; 28:7324–7333. [PubMed: 18632936]

Amaral, D.; Lavenex, P. Hippocampal Neuroanatomy. In: Andersen, P.; Morris, R.; Amaral, D.; Bliss, TVP.; O’Keefe, J., editors. The Hippocampus Book. New York, NY: Oxford University Press; 2007. p. 37-114.

Amaral DG, Witter MP. The three-dimensional organization of the hippocampal formation: A review of anatomical data. Neuroscience. 1989; 31:571–591. [PubMed: 2687721]

Andreasen M, Lambert JD. Regenerative properties of pyramidal cell dendrites in area CA1 of the rat hippocampus. J Physiol. 1995; 483(Pt 2):421–441. [PubMed: 7650611]

Azouz R, Jensen MS, Yaari Y. Ionic basis of spike after-depolarization and burst generation in adult rat hippocampal CA1 pyramidal cells. J Physiol. 1996; 492(Pt 1):211–223. [PubMed: 8730596]

NIH-PA Author Manuscript

NIH-PA Author Manuscript

NIH-PA Author Manuscript

Barnes CA, McNaughton BL, Mizumori SJ, Leonard BW, Lin LH. Comparison of spatial and temporal characteristics of neuronal activity in sequential stages of hippocampal processing. Prog Brain Res. 1990; 83:287–300. [PubMed: 2392566]

Bostock E, Muller RU, Kubie JL. Experience-dependent modifications of hippocampal place cell firing. Hippocampus. 1991; 1:193–205. [PubMed: 1669293]

Buzsaki G, Leung LW, Vanderwolf CH. Cellular bases of hippocampal EEG in the behaving rat. Brain Res. 1983; 287:139–171. [PubMed: 6357356]

Buzsaki G, Horvath Z, Urioste R, Hetke J, Wise K. High-frequency network oscillation in the hippocampus. Science. 1992; 256:1025–1027. [PubMed: 1589772]

Chevaleyre V, Siegelbaum SA. Strong CA2 pyramidal neuron synapses define a powerful disynaptic cortico-hippocampal loop. Neuron. 2010; 66:560–572. [PubMed: 20510860]

Csicsvari J, Hirase H, Czurko A, Mamiya A, Buzsaki G. Oscillatory coupling of hippocampal pyramidal cells and interneurons in the behaving Rat. J Neurosci. 1999; 19:274–287. [PubMed: 9870957]

Csicsvari J, Hirase H, Mamiya A, Buzsaki G. Ensemble patterns of hippocampal CA3-CA1 neurons during sharp wave-associated population events. Neuron. 2000; 28:585–594. [PubMed: 11144366]

Debanne D, Gahwiler BH, Thompson SM. Long-term synaptic plasticity between pairs of individual CA3 pyramidal cells in rat hippocampal slice cultures. J Physiol. 1998; 507(Pt 1):237–247. [PubMed: 9490845]

Derdikman D, Whitlock JR, Tsao A, Fyhn M, Hafting T, Moser MB, Moser EI. Fragmentation of grid cell maps in a multicom-partment environment. Nat Neurosci. 2009; 12:1325–1332. [PubMed: 19749749]

Diba K, Buzsaki G. Hippocampal network dynamics constrain the time lag between pyramidal cells across modified environments. J Neurosci. 2008; 28:13448–13456. [PubMed: 19074018]

Dragoi G, Buzsaki G. Temporal encoding of place sequences by hippocampal cell assemblies. Neuron. 2006; 50:145–157. [PubMed: 16600862]

Eichenbaum H, Dudchenko P, Wood E, Shapiro M, Tanila H. The hippocampus, memory, and place cells: Is it spatial memory or a memory space? Neuron. 1999; 23:209–226. [PubMed: 10399928]

Ferbinteanu J, Shapiro ML. Prospective and retrospective memory coding in the hippocampus. Neuron. 2003; 40:1227–1239. [PubMed: 14687555]

Frank LM, Brown EN, Wilson M. Trajectory encoding in the hippocampus and entorhinal cortex. Neuron. 2000; 27:169–178. [PubMed: 10939340]

Gasparini S, Migliore M, Magee JC. On the initiation and propagation of dendritic spikes in CA1 pyramidal neurons. J Neurosci. 2004; 24:11046–11056. [PubMed: 15590921]

Gill PR, Mizumori SJ, Smith DM. Hippocampal episode fields develop with learning. Hippocampus. 2010; 21:1240–1249. [PubMed: 20665593]

Golding NL, Spruston N. Dendritic sodium spikes are variable triggers of axonal action potentials in hippocampal CA1 pyramidal neurons. Neuron. 1998; 21:1189–1200. [PubMed: 9856473]

Golding NL, Kath WL, Spruston N. Dichotomy of action-potential backpropagation in CA1 pyramidal neuron dendrites. J Neurophysiol. 2001; 86:2998–3010. [PubMed: 11731556]

Golding NL, Staff NP, Spruston N. Dendritic spikes as a mechanism for cooperative long-term potentiation. Nature. 2002; 418:326–331. [PubMed: 12124625]

Gothard KM, Skaggs WE, Moore KM, McNaughton BL. Binding of hippocampal CA1 neural activity to multiple reference frames in a landmark-based navigation task. J Neurosci. 1996; 16:823–835. [PubMed: 8551362]

Guzowski JF, Knierim JJ, Moser EI. Ensemble dynamics of hippocampal regions CA3 and CA1. Neuron. 2004; 44:581–584. [PubMed: 15541306]

Hafting T, Fyhn M, Molden S, Moser MB, Moser EI. Micro-structure of a spatial map in the entorhinal cortex. Nature. 2005; 436:801–806. [PubMed: 15965463]

Hafting T, Fyhn M, Bonnevie T, Moser MB, Moser EI. Hippocampus-independent phase precession in entorhinal grid cells. Nature. 2008; 453:1248–1252. [PubMed: 18480753]

NIH-PA Author Manuscript NIH-PA Author Manuscript NIH-PA Author Manuscript

Harris KD, Henze DA, Csicsvari J, Hirase H, Buzsaki G. Accuracy of tetrode spike separation as determined by simultaneous intracellular and extracellular measurements. J Neurophysiol. 2000; 84:401–414. [PubMed: 10899214]

Harris KD, Hirase H, Leinekugel X, Henze DA, Buzsaki G. Temporal interaction between single spikes and complex spike bursts in hippocampal pyramidal cells. Neuron. 2001; 32:141–149. [PubMed: 11604145]

Hazan L, Zugaro M, Buzsaki G. Klusters, NeuroScope, NDManager: A free software suite for neurophysiological data processing and visualization. J Neurosci Methods. 2006; 155:207–216. [PubMed: 16580733]

Henriksen EJ, Colgin LL, Barnes CA, Witter MP, Moser MB, Moser EI. Spatial representation along the proximodistal axis of CA1. Neuron. 2010; 68:127–137. [PubMed: 20920796]

Hok V, Lenck-Santini PP, Roux S, Save E, Muller RU, Poucet B. Goal-related activity in hippocampal place cells. J Neurosci. 2007; 27:472–482. [PubMed: 17234580]

Hu H, Vervaeke K, Storm JF. Two forms of electrical resonance at theta frequencies, generated by M-current, h-current and persistent Na+ current in rat hippocampal pyramidal cells. J Physiol. 2002; 545:783–805. [PubMed: 12482886]

Hu H, Vervaeke K, Graham LJ, Storm JF. Complementary theta resonance filtering by two spatially segregated mechanisms in CA1 hippocampal pyramidal neurons. J Neurosci. 2009; 29:14472–14483. [PubMed: 19923281]

Ishizuka N, Weber J, Amaral DG. Organization of intrahippocampal projections originating from CA3 pyramidal cells in the rat. J Comp Neurol. 1990; 295:580–623. [PubMed: 2358523]

Huxter J, Burgess N, O'Keefe J. Independent rate and temporal coding in hippocampal pyramidal cells. Nature. 2003; 425:828–832. [PubMed: 14574410]

Jarsky T, Roxin A, Kath WL, Spruston N. Conditional dendritic spike propagation following distal synaptic activation of hippocampal CA1 pyramidal neurons. Nat Neurosci. 2005; 8:1667–1676. [PubMed: 16299501]

Jonas P, Major G, Sakmann B. Quantal components of unitary EPSCs at the mossy fibre synapse on CA3 pyramidal cells of rat hippocampus. J Physiol. 1993; 472:615–663. [PubMed: 7908327]

Jones MW, McHugh TJ. Updating hippocampal representations: CA2 joins the circuit. Trends Neurosci. 2011; 34:526–535. [PubMed: 21880379]

Jung HY, Mickus T, Spruston N. Prolonged sodium channel inactivation contributes to dendritic action potential attenuation in hippocampal pyramidal neurons. J Neurosci. 1997; 17:6639–6646. [PubMed: 9254676]

Kamondi A, Acsady L, Buzsaki G. Dendritic spikes are enhanced by cooperative network activity in the intact hippocampus. J Neurosci. 1998; 18:3919–3928. [PubMed: 9570819]

Kjelstrup KB, Solstad T, Brun VH, Hafting T, Leutgeb S, Witter MP, Moser EI, Moser MB. Finite scale of spatial representation in the hippocampus. Science. 2008; 321:140–143. [PubMed: 18599792]

Knierim JJ. Dynamic interactions between local surface cues, distal landmarks, and intrinsic circuitry in hippocampal place cells. J Neurosci. 2002; 22:6254–6264. [PubMed: 12122084]

Kobayashi K, Poo MM. Spike train timing-dependent associative modification of hippocampal CA3 recurrent synapses by mossy fibers. Neuron. 2004; 41:445–454. [PubMed: 14766182]

Larkum ME, Zhu JJ, Sakmann B. A new cellular mechanism for coupling inputs arriving at different cortical layers. Nature. 1999; 398:338–341. [PubMed: 10192334]

Lee I, Knierim JJ. The relationship between the field-shifting phenomenon and representational coherence of place cells in CA1 and CA3 in a cue-altered environment. Learn Mem. 2007; 14:807–815. [PubMed: 18007023]

Lee I, Yoganarasimha D, Rao G, Knierim JJ. Comparison of population coherence of place cells in hippocampal subfields CA1 and CA3. Nature. 2004a; 430:456–459. [PubMed: 15229614]

Lee I, Rao G, Knierim JJ. A double dissociation between hippocampal subfields: Differential time course of CA3 and CA1 place cells for processing changed environments. Neuron. 2004b; 42:803–815. [PubMed: 15182719]

Leung LS. A model of intracellular model of intracellular θ phase precession dependent on intrinsic subthreshold membrane currents. J Neurosci. 2011; 31:12282–12296. [PubMed: 21865471]

NIH-PA Author Manuscript

NIH-PA Author Manuscript

NIH-PA Author Manuscript

Leung LS, Yu HW. Theta-frequency resonance in hippocampal CA1 neurons in vitro demonstrated by sinusoidal current injection. J Neurophysiol. 1998; 79:1592–1596. [PubMed: 9497437]

Leutgeb S, Leutgeb JK. Pattern separation, pattern completion, and new neuronal codes within a continuous CA3 map. Learn Mem. 2007; 14:745–757. [PubMed: 18007018]

Leutgeb S, Leutgeb JK, Treves A, Moser MB, Moser EI. Distinct ensemble codes in hippocampal areas CA3 and CA1. Science. 2004; 305:1295–1298. [PubMed: 15272123]

Leutgeb JK, Leutgeb S, Treves A, Meyer R, Barnes CA, McNaughton BL, Moser MB, Moser EI. Progressive transformation of hippocampal neuronal representations in “morphed” environments. Neuron. 2005; 48:345–358. [PubMed: 16242413]

Li XG, Somogyi P, Ylinen A, Buzsaki G. The hippocampal CA3 network: An in vivo intracellular labeling study. J Comp Neurol. 1994; 339:181–208. [PubMed: 8300905]

Losonczy A, Makara JK, Magee JC. Compartmentalized dendritic plasticity and input feature storage in neurons. Nature. 2008; 452:436–441. [PubMed: 18368112]

Magee JC, Carruth M. Dendritic voltage-gated ion channels regulate the action potential firing mode of hippocampal CA1 pyramidal neurons. J Neurophysiol. 1999; 82:1895–1901. [PubMed: 10515978]

Magee JC, Johnston D. A synaptically controlled, associative signal for Hebbian plasticity in hippocampal neurons. Science. 1997; 275:209–213. [PubMed: 8985013]

Major G, Larkman AU, Jonas P, Sakmann B, Jack JJ. Detailed passive cable models of whole-cell recorded CA3 pyramidal neurons in rat hippocampal slices. J Neurosci. 1994; 14:4613–4638. [PubMed: 8046439]

Markus EJ, Barnes CA, McNaughton BL, Gladden VL, Skaggs WE. Spatial information content and reliability of hippocampal CA1 neurons: Effects of visual input. Hippocampus. 1994; 4:410–421. [PubMed: 7874233]

Maurer AP, Vanrhoads SR, Sutherland GR, Lipa P, McNaughton BL. Self-motion and the origin of differential spatial scaling along the septo-temporal axis of the hippocampus. Hippocampus. 2005; 15:841–852. [PubMed: 16145692]

McNaughton BL, Morris RGM. Hippocampal synaptic enhancement and information storage within a distributed memory system. Trend Neurosci. 1987; 10:408–415.

McMahon DB, Barrionuevo G. Short- and long-term plasticity of the perforant path synapse in hippocampal area CA3. J Neurophysiol. 2002; 88:528–533. [PubMed: 12091576]

McNaughton BL, Barnes CA, O’Keefe J. The contributions of position, direction, and velocity to single unit activity in the hippocampus of freely-moving rats. Exp Brain Res. 1983; 52:41–49. [PubMed: 6628596]

McNaughton BL, Barnes CA, Gerrard JL, Gothard K, Jung MW, Knierim JJ, Kudrimoti H, Qin Y, Skaggs WE, Suster M, Weaver KL. Deciphering the hippocampal polyglot: The hippocampus as a path integration system. J Exp Biol. 1996; 199:173–185. [PubMed: 8576689]

McNaughton BL, Battaglia FP, Jensen O, Moser EI, Moser MB. Path integration and the neural basis of the ‘cognitive map’. Nat Rev Neurosci. 2006; 7:663–678. [PubMed: 16858394]

Meeks JP, Mennerick S. Action potential initiation and propagation in CA3 pyramidal axons. J Neurophysiol. 2007; 97:3460–3472. [PubMed: 17314237]

Mehta MR, Barnes CA, McNaughton BL. Experience-dependent, asymmetric expansion of hippocampal place fields. Proc Natl Acad Sci USA. 1997; 94:8918–8921. [PubMed: 9238078]

Metzner W, Koch C, Wessel R, Gabbiani F. Feature extraction by burst-like spike patterns in multiple sensory maps. J Neurosci. 1998; 18:2283–2300. [PubMed: 9482813]

Mickus T, Jung H, Spruston N. Properties of slow, cumulative sodium channel inactivation in rat hippocampal CA1 pyramidal neurons. Biophys J. 1999; 76:846–860. [PubMed: 9929486]

Mizuseki K, Sirota A, Pastalkova E, Buzsaki G. Theta oscillations provide temporal windows for local circuit computation in the entorhinal-hippocampal loop. Neuron. 2009; 64:267–280. [PubMed: 19874793]

Mizuseki K, Diba K, Pastalkova E, Buzsaki G. Hippocampal CA1 pyramidal cells form functionally distinct sublayers. Nat Neurosci. 2011; 14:1174–1181. [PubMed: 21822270]

NIH-PA Author Manuscript

NIH-PA Author Manuscript

NIH-PA Author Manuscript

Montgomery SM, Sirota A, Buzsaki G. Theta and gamma coordination of hippocampal networks during waking and rapid eye movement sleep. J Neurosci. 2008; 28:6731–6741. [PubMed: 18579747]

Moser EI, Kropff E, Moser MB. Place cells, grid cells, and the brain's spatial representation system. Annu Rev Neurosci. 2008; 31:69–89. [PubMed: 18284371]

Muller RU, Kubie JL. The effects of changes in the environment on the spatial firing of hippocampal complex-spike cells. J Neurosci. 1987; 7:1951–1968. [PubMed: 3612226]

Muller RU, Kubie JL. The firing of hippocampal place cells predicts the future position of freely moving rats. J Neurosci. 1989; 9:4101–4110. [PubMed: 2592993]

Nitz DA. Path shape impacts the extent of CA1 pattern recurrence both within and across environments. J Neurophysiol. 2011; 105:1815–1824. [PubMed: 21289139]

O'Keefe J, Burgess N. Geometric determinants of the place fields of hippocampal neurons. Nature. 1996; 381:425–428. [PubMed: 8632799]

O'Keefe, J.; Nadel, L. The Hippocampus as a Cognitive Map. Oxford: Oxford University Press; 1978.

O'Keefe J, Recce ML. Phase relationship between hippocampal place units and the EEG theta rhythm. Hippocampus. 1993; 3:317–330. [PubMed: 8353611]

O'Keefe J, Speakman A. Single unit activity in the rat hippocampus during a spatial memory task. Exp Brain Res. 1987; 68:1–27. [PubMed: 3691688]

Olton DS, Becker JT, Handelmann GE. Hippocampus, space, and memory. Behav Brain Sci. 1979; 2:313–365.

O'Reilly RC, McClelland JL. Hippocampal conjunctive encoding, storage, and recall: Avoiding a trade-off. Hippocampus. 1994; 4:661–682. [PubMed: 7704110]

Park E, Dvorak D, Fenton AA. Ensemble place codes in hippocampus: CA1, CA3, and dentate gyrus place cells have multiple place fields in large environments. PLoS One. 2011; 6:e22349. [PubMed: 21789250]

Pastalkova E, Itskov V, Amarasingham A, Buzsaki G. Internally generated cell assembly sequences in the rat hippocampus. Science. 2008; 321:1322–1327. [PubMed: 18772431]

Paz-Villagran V, Save E, Poucet B. Independent coding of connected environments by place cells. Eur J Neurosci. 2004; 20:1379–1390. [PubMed: 15341610]

Pelkey KA, McBain CJ. Target-cell-dependent plasticity within the mossy fibre-CA3 circuit reveals compartmentalized regulation of presynaptic function at divergent release sites. J Physiol. 2008; 586:1495–1502. [PubMed: 18079156]

Pike FG, Goddard RS, Suckling JM, Ganter P, Kasthuri N, Paulsen O. Distinct frequency preferences of different types of rat hippocampal neurones in response to oscillatory input currents. J Physiol. 2000; 529(Pt 1):205–213. [PubMed: 11080262]

Pinsky PF, Rinzel J. Intrinsic and network rhythmogenesis in a reduced Traub model for CA3 neurons. J Comput Neurosci. 1994; 1:39–60. [PubMed: 8792224]

Poirazi P, Mel BW. Impact of active dendrites and structural plasticity on the memory capacity of neural tissue. Neuron. 2001; 29:779–796. [PubMed: 11301036]

Ranck JB Jr. Studies on single neurons in dorsal hippocampal formation and septum in unrestrained rats. I. Behavioral correlates and firing repertoires. Exp Neurol. 1973; 41:461–531. [PubMed: 4355646]

Rolls ET, Kesner RP. A computational theory of hippocampal function, and empirical tests of the theory. Prog Neurobiol. 2006; 79:1–48. [PubMed: 16781044]

Rotstein HG, Pervouchine DD, Acker CD, Gillies MJ, White JA, Buhl EH, Whittington MA, Kopell N. Slow and fast inhibition and an H-current interact to create a theta rhythm in a model of CA1 interneuron network. J Neurophysiol. 2005; 94:1509–1518. [PubMed: 15857967]

Royer S, Sirota A, Patel J, Buzsaki G. Distinct representations and theta dynamics in dorsal and ventral hippocampus. J Neurosci. 2010; 30:1777–1787. [PubMed: 20130187]

Sargolini F, Fyhn M, Hafting T, McNaughton BL, Witter MP, Moser MB, Moser EI. Conjunctive representation of position, direction, and velocity in entorhinal cortex. Science. 2006; 312:758–762. [PubMed: 16675704]

NIH-PA Author Manuscript

NIH-PA Author Manuscript

NIH-PA Author Manuscript

Sirota A, Montgomery S, Fujisawa S, Isomura Y, Zugaro M, Buzsaki G. Entrainment of neocortical neurons and gamma oscillations by the hippocampal theta rhythm. Neuron. 2008; 60:683–697. [PubMed: 19038224]

Skaggs WE, McNaughton BL. Spatial firing properties of hippocampal CA1 populations in an environment containing two visually identical regions. J Neurosci. 1998; 18:8455–8466. [PubMed: 9763488]

Skaggs, WE.; McNaughton, BL.; Gothard, KM.; Markus, EJ. An information-theoretic approach to deciphering the hippocampal code. In: Hanson, SJ.; Cowan, JD.; Giles, CL., editors. Advances in Neural Information Processing Systems. Vol. vol. 5. San Francisco, CA: Morgan Kaufmann; 1993. p. 1030-1037.

Skaggs WE, McNaughton BL, Wilson MA, Barnes CA. Theta phase precession in hippocampal neuronal populations and the compression of temporal sequences. Hippocampus. 1996; 6:149–172. [PubMed: 8797016]

Solstad T, Boccara CN, Kropff E, Moser MB, Moser EI. Representation of geometric borders in the entorhinal cortex. Science. 2008; 322:1865–1868. [PubMed: 19095945]

Spruston N. Pyramidal neurons: Dendritic structure and synaptic integration. Nat Rev Neurosci. 2008; 9:206–221. [PubMed: 18270515]

Spruston N, Schiller Y, Stuart G, Sakmann B. Activity-dependent action potential invasion and calcium influx into hippocampal CA1 dendrites. Science. 1995a; 268:297–300. [PubMed: 7716524]

Spruston N, Jonas P, Sakmann B. Dendritic glutamate receptor channels in rat hippocampal CA3 and CA1 pyramidal neurons. J Physiol. 1995b; 482(Pt 2):325–352. [PubMed: 7536248]

Squire LR. Memory and the hippocampus: A synthesis from findings with rats, monkeys, and humans. Psychol Rev. 1992; 99:195–231. [PubMed: 1594723]

Su H, Alroy G, Kirson ED, Yaari Y. Extracellular calcium modulates persistent sodium current-dependent burst-firing in hippocampal pyramidal neurons. J Neurosci. 2001; 21:4173–4182. [PubMed: 11404402]

Takahashi H, Magee JC. Pathway interactions and synaptic plasticity in the dendritic tuft regions of CA1 pyramidal neurons. Neuron. 2009; 62:102–111. [PubMed: 19376070]

Tanila H. Hippocampal place cells can develop distinct representations of two visually identical environments. Hippocampus. 1999; 9:235–246. [PubMed: 10401639]

Taube JS. The head direction signal: Origins and sensory-motor integration. Annu Rev Neurosci. 2007; 30:181–207. [PubMed: 17341158]

Traub RD, Wong RK, Miles R, Michelson H. A model of a CA3 hippocampal pyramidal neuron incorporating voltage-clamp data on intrinsic conductances. J Neurophysiol. 1991; 66:635–650. [PubMed: 1663538]

Traub RD, Jefferys JG, Miles R, Whittington MA, Toth K. A branching dendritic model of a rodent CA3 pyramidal neurone. J Physiol. 1994; 481(Pt 1):79–95. [PubMed: 7853251]

Turner DA, Li XG, Pyapali GK, Ylinen A, Buzsaki G. Morphometric and electrical properties of reconstructed hippocampal CA3 neurons recorded in vivo. J Comp Neurol. 1995; 356:580–594. [PubMed: 7560268]

Vazdarjanova A, Guzowski JF. Differences in hippocampal neuronal population responses to modifications of an environmental context: Evidence for distinct, yet complementary, functions of CA3 and CA1 ensembles. J Neurosci. 2004; 24:6489–6496. [PubMed: 15269259]

Wills TJ, Lever C, Cacucci F, Burgess N, O'Keefe J. Attractor dynamics in the hippocampal representation of the local environment. Science. 2005; 308:873–876. [PubMed: 15879220]

Wong RK, Prince DA. Afterpotential generation in hippocampal pyramidal cells. J Neurophysiol. 1981; 45:86–97. [PubMed: 6259299]

Wood ER, Dudchenko PA, Robitsek RJ, Eichenbaum H. Hippocampal neurons encode information about different types of memory episodes occurring in the same location. Neuron. 2000; 27:623–633. [PubMed: 11055443]

Yue C, Yaari Y. KCNQ/M channels control spike afterdepolarization and burst generation in hippocampal neurons. J Neurosci. 2004; 24:4614–4624. [PubMed: 15140933]

NIH-PA Author Manuscript
NIH-PA Author Manuscript
NIH-PA Author Manuscript

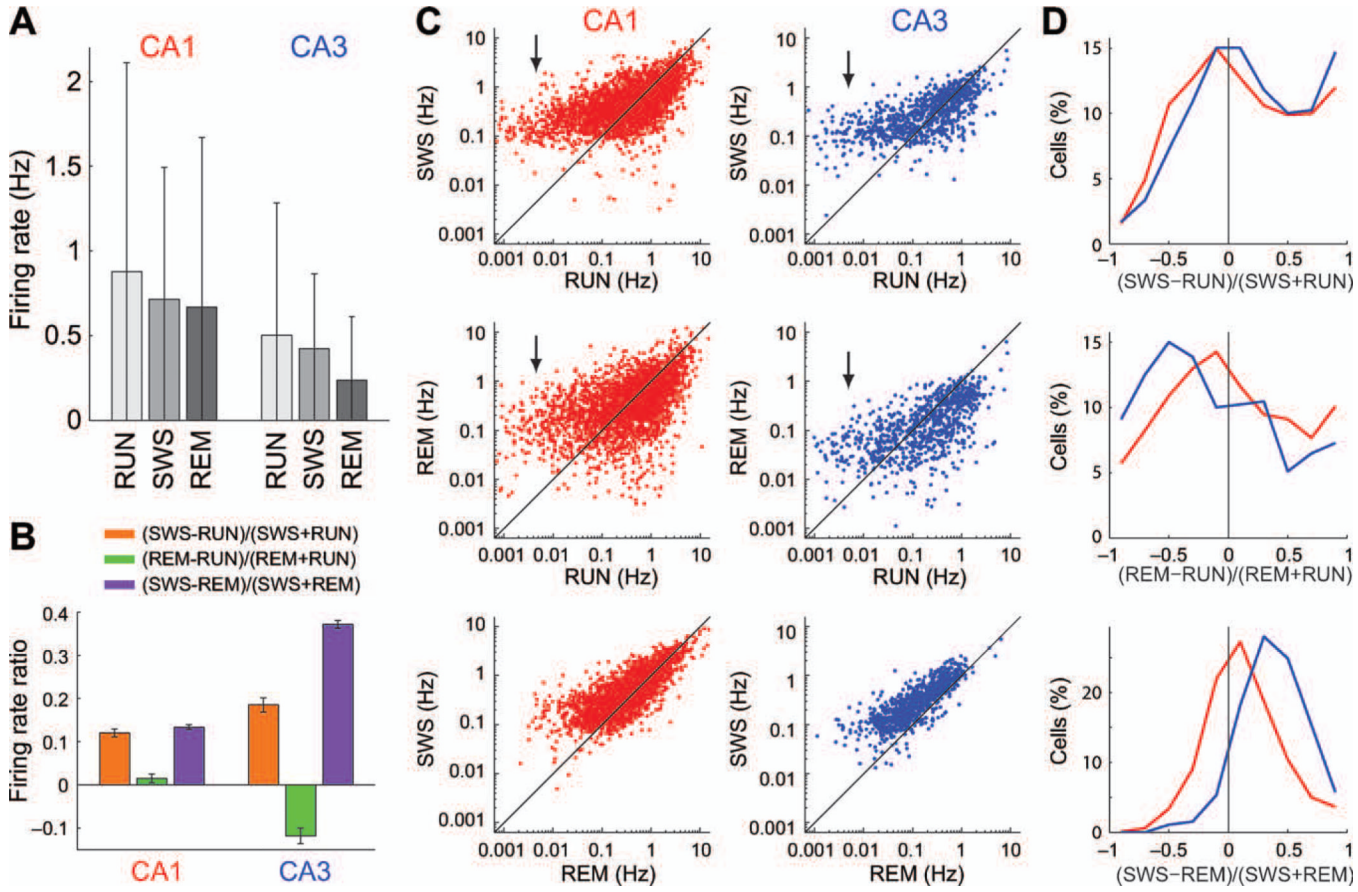

FIGURE 1.

Brain state-dependent changes of firing rates of CA1 and CA3 pyramidal cells. A: Firing rate comparison of CA1 and CA3 pyramidal cells in different brain states. SWS, slow wave sleep; REM, rapid eye movement sleep; RUN, task-related ambulation. mean firing rates ± SD. B: Firing rate ratios across behavioral. Mean ± SEM. C: Rate shifts of neurons across states. Each dot is a single neuron. Arrows point to “silent” cells (<0.01 Hz) during RUN. D: Distributions of firing rate shift between different brain states. Red, CA1; Blue, CA3 in (A), (C), and (D). [Color figure can be viewed in the online issue, which is available at wileyonlinelibrary.com.]

NIH-PA Author Manuscript

NIH-PA Author Manuscript

NIH-PA Author Manuscript

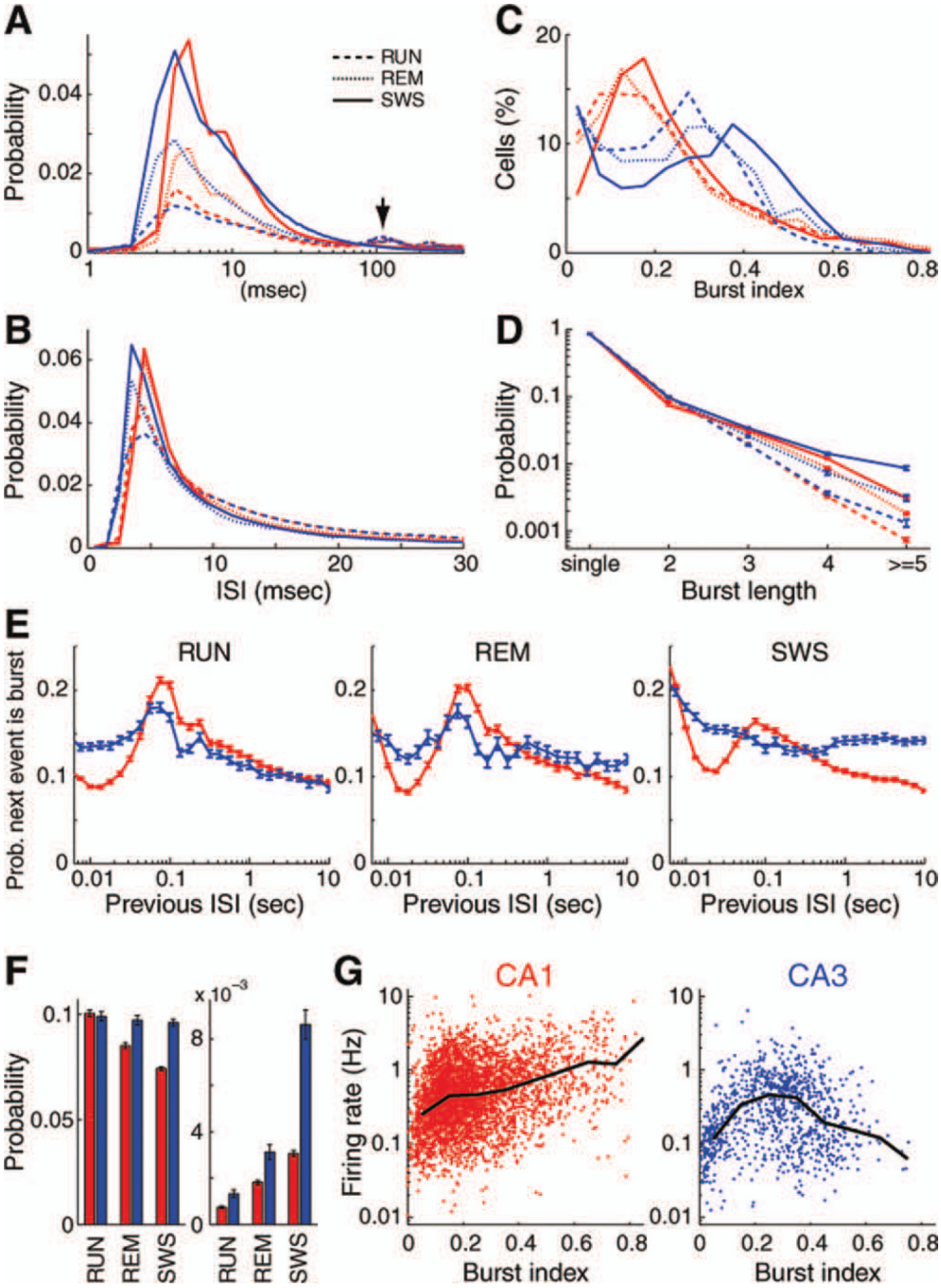

FIGURE 2.

Single spike and burst discharge properties of CA1 and CA3 pyramidal neurons. Mean autocorrelograms (A) and interspike interval histograms (B) of CA1 and CA3 pyramidal neurons in RUN, REM, and SWS states. Arrow, peak at theta frequency during RUN and REM. Bin size: 1 ms. In (A), probability for each neuron was normalized such that sum of the probability between 1 to 400 msec is unity. C: Histograms of burst index. Note stronger behavior dependence and higher propensity of spike bursts in CA3 than CA1 neurons. D: Probability distribution of burst lengths. Note supraexponential distribution for both groups in SWS and REM and the higher incidence of longer bursts in CA3 neurons. E: Burst event probability (two spikes or more) as a function of preceding silent (nonspiking) period. Note

NIH-PA Author Manuscript

NIH-PA Author Manuscript

NIH-PA Author Manuscript

peaks at ~ 100 ms in CA1 neurons in all states. Note also that peaks occur at slightly shorter intervals for CA3 than CA1 pyramidal neurons during RUN and REM. F: Fraction of bursts (relative to all events) in different brain states. Left, burst length = 2 spikes (doublets). Right, burst length five or more spikes. Note state dependence of bursts in both CA1 and CA3 neurons and higher probability of long bursts in CA3 pyramidal cells. Same data as in Figure 2D. G: Relationship between the burst index and the firing rate of neurons. Burst index and firing rate were calculated using all the data regardless of brain states. Each dot is a single neuron. Note monotonic relationship between the mean firing rate and burst index of CA1 pyramidal cells and the inverted-U relationship for CA3 cells. Black lines represent running medians. Red, CA1; Blue, CA3 in all panels. [Color figure can be viewed in the online issue, which is available at wileyonlinelibrary.com.]

NIH-PA Author Manuscript
NIH-PA Author Manuscript
NIH-PA Author Manuscript

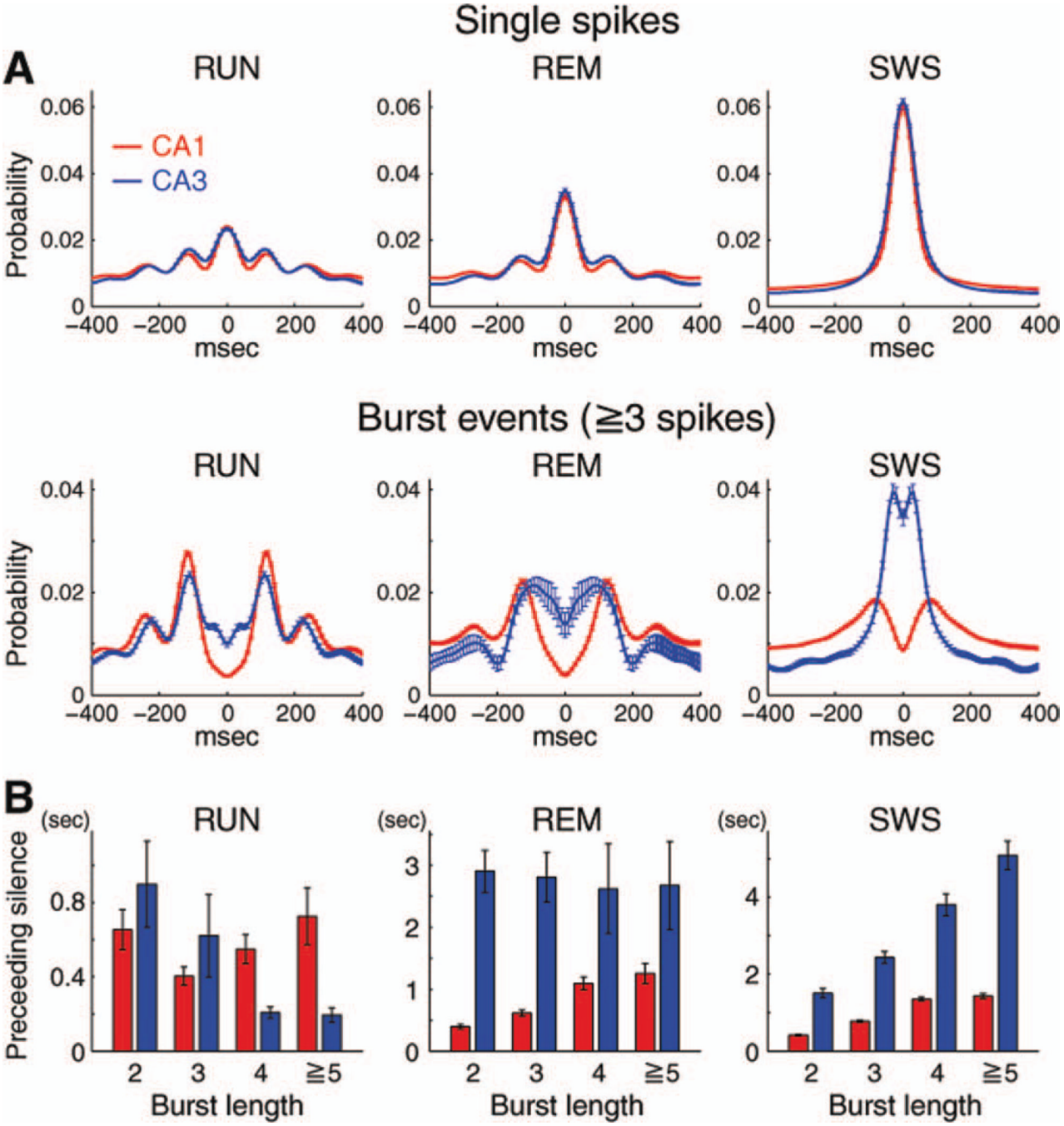

FIGURE 3.

Single spike versus burst dynamics of CA1 and CA3 pyramidal neurons. A: Autocorrelograms of single spikes (ISI > 6 ms, top row) and burst events (three or more spikes) in different brain states. Note peaks of burst patterns at ~ 100 ms in CA1 neurons in all three states. Probability for each neuron was normalized such that the total of the probability between −400 and 400 msec was unity, and mean ± SEM are shown. B: Length of spike-preceding silent periods as a function of burst length. Mean ± SEM of medians are shown. Note that spiking history and state differentially affect CA1 and CA3 pyramidal neurons. Red, CA1; Blue, CA3 in all panels. [Color figure can be viewed in the online issue, which is available at wileyonlinelibrary.com.]

NIH-PA Author Manuscript

NIH-PA Author Manuscript

NIH-PA Author Manuscript

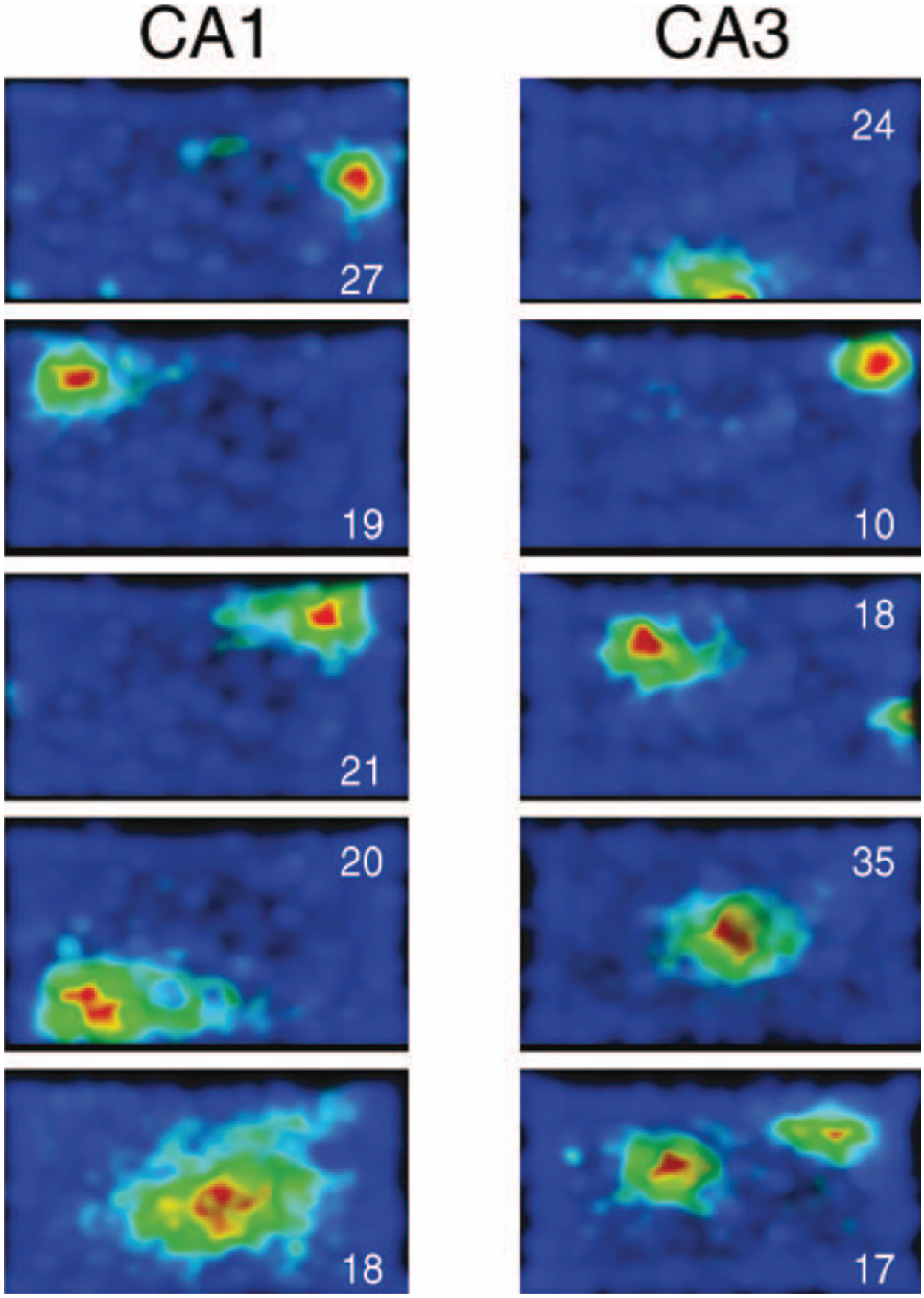

FIGURE 4.

Example place cells in the open field. Heatmaps show position-related firing rates of different neurons in CA1 and CA3 pyramidal layers. Numbers indicate peak firing rates (Hz). Size of the open field is 200 × 100 cm^2. [Color figure can be viewed in the online issue, which is available at wileyonlinelibrary.com.]

NIH-PA Author Manuscript
NIH-PA Author Manuscript
NIH-PA Author Manuscript

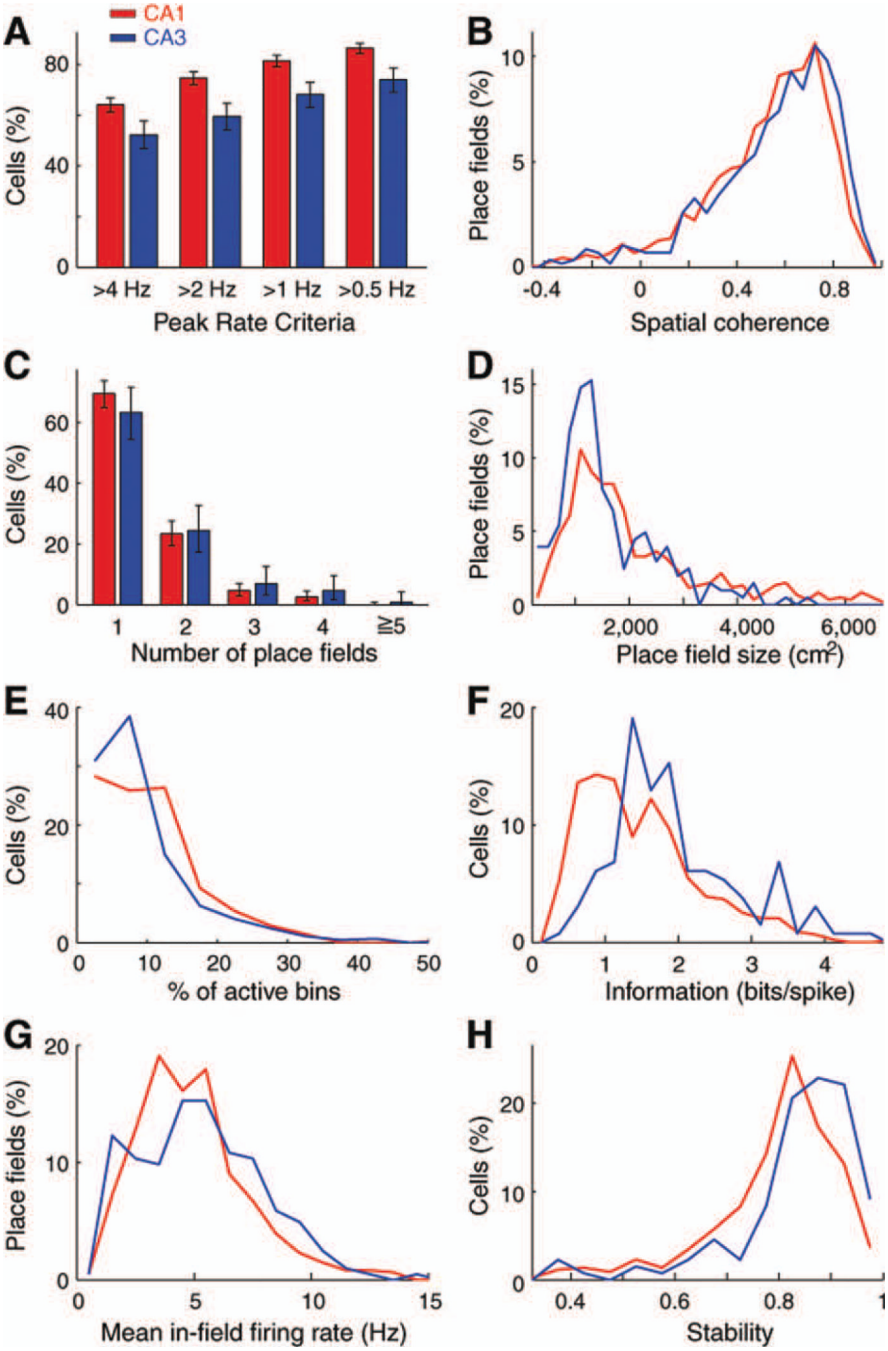

FIGURE 5.

Spatial features of CA1 and CA3 pyramidal neurons on the open field. A: Fraction of CA1 (red) and CA3 (blue) neurons with place fields, determined by peak firing rates from >0.5 Hz to >4 Hz. B: Distribution of the spatial coherence for neurons with >2 Hz peak firing rates in the place field. For parts (C–H), only neurons with place fields with >2 Hz peak and >0.7 spatial coherence are included. C: Number of place fields. D: Place field size. E: Number or active pixels (i.e., area coverage) defined by pixels with >20% of the peak firing rate. F: Information (bits/spike). G: Average within- field firing rate. H: Stability defined as the pixel-by-pixel correlation of firing rates between the first and second halves of trials in a session. All comparisons but the number of place fields and in-field firing rate are

NIH-PA Author Manuscript

NIH-PA Author Manuscript

NIH-PA Author Manuscript

significantly different ($P < 0.01$) between CA1 and CA3 pyramidal cells. Red, CA1; Blue, CA3 in all panels. Size of the open field was 180 × 180 cm^2, except for E, where 200 × 100 cm^2 field was used. In (A) and (C), ± 95% Clopper-Pearson confidential intervals are shown. [Color figure can be viewed in the online issue, which is available at wileyonlinelibrary.com.]

NIH-PA Author Manuscript

NIH-PA Author Manuscript

NIH-PA Author Manuscript

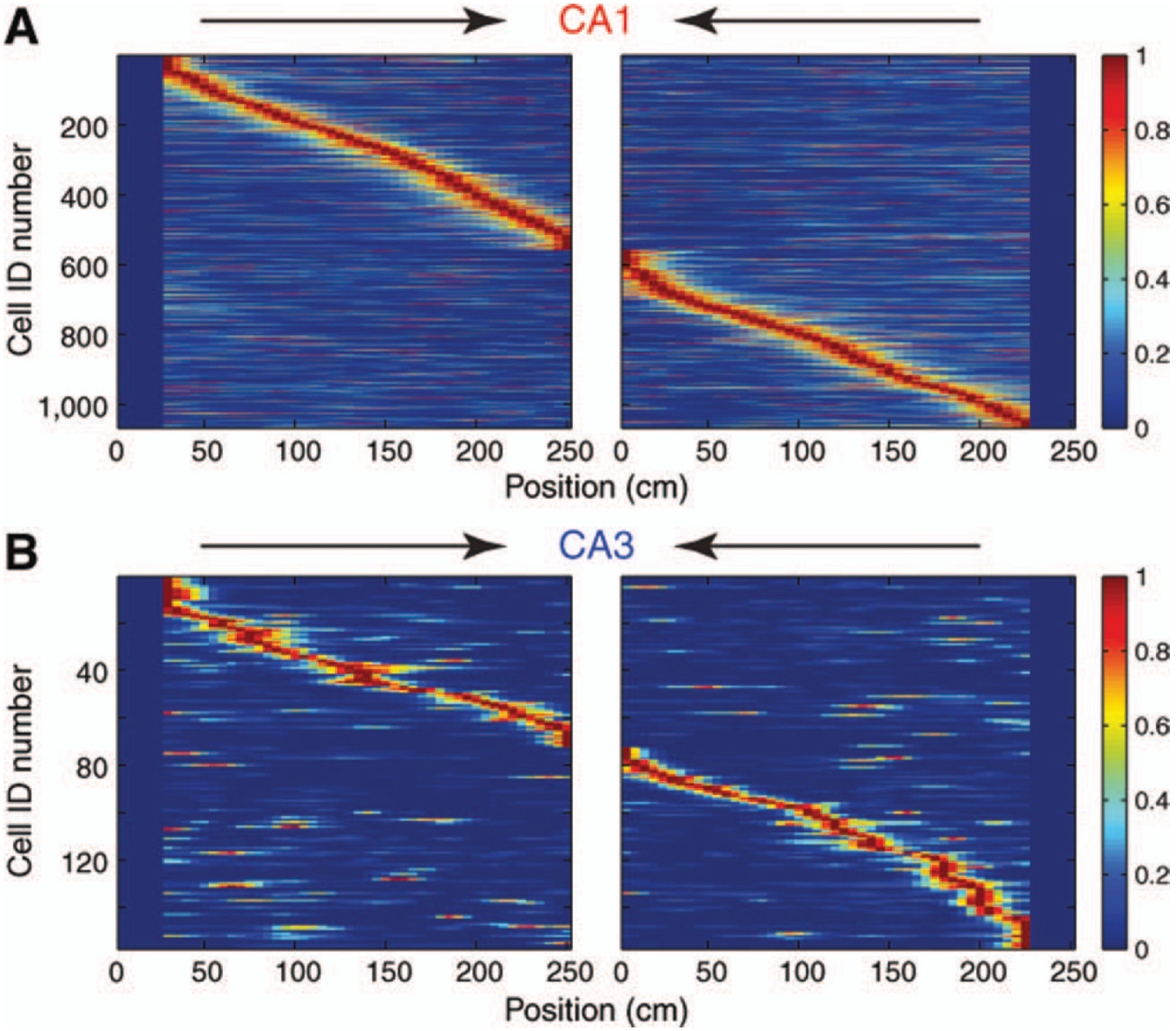

FIGURE 6.

Context-dependent firing patterns in CA1 and CA3 pyramidal cells on the linear track. Color-coded, normalized firing rates of CA1 and CA3 pyramidal cells during left and right journeys (cell-identify is the same). Each line represents a single cell. 1 (red) = peak firing rate. Note strongly different firing rates of the same neuron during left and right traverses. [Color figure can be viewed in the online issue, which is available at wileyonlinelibrary.com.]

NIH-PA Author Manuscript

NIH-PA Author Manuscript

NIH-PA Author Manuscript

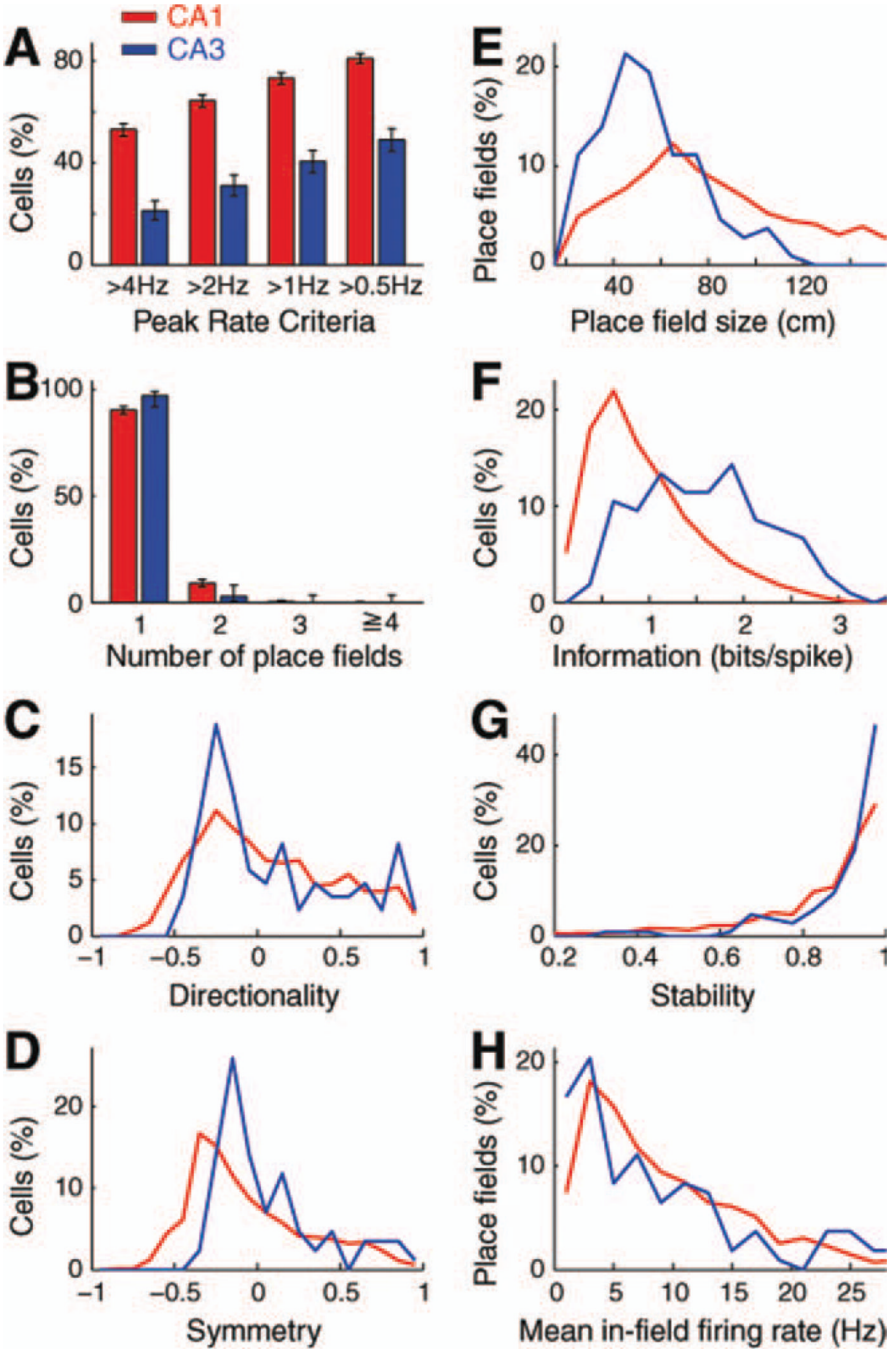

FIGURE 7.

Spatial features of CA1 and CA3 pyramidal neurons on the linear track. A: Fraction of CA1 (red) and CA3 (blue) neurons with place fields, defined by peak firing from >0.5 Hz to >4 Hz. B: Number of place fields. ±95% Clopper-Pearson confidence intervals are shown in (A) and (B). C: Directionality index defined as the pixel-by-pixel correlation of firing rate map during left versus righ travels. This relationship provides information about the strength of rate-position relationship of a neuron, when position is referenced to distant (room) cues (Gothard et al., 1996). D: Symmetry index defined as the pixel-by-pixel correlation of firing rate map during left versus *reversed* (mirrored) right travels. This relationship provides information about the strength of rate-position relationship of a neuron, when position is

NIH-PA Author Manuscript

NIH-PA Author Manuscript

NIH-PA Author Manuscript

referenced to the start (or finish) point (Gothard et al., 1996). E: Place field size. F: Information (bits/spike). G: Stability. H: Average in-field firing rate. All comparisons but the number of place fields, directionality index and in-field firing rate are significantly different ($P < 0.01$) between CA1 and CA3 pyramidal cells. Red, CA1; Blue, CA3 in all panels. [Color figure can be viewed in the online issue, which is available at wileyonlinelibrary.com.]

NIH-PA Author Manuscript
NIH-PA Author Manuscript
NIH-PA Author Manuscript

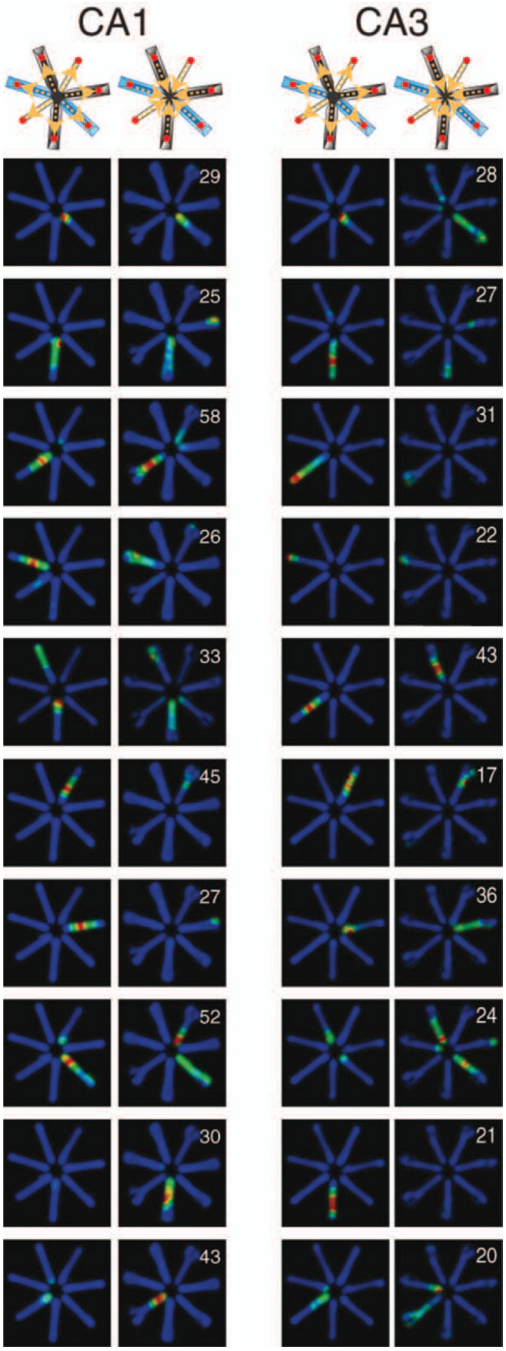

FIGURE 8.
Example place cells in the radial arm maze. Heatmaps show position-related firing rates of representative CA1 and CA3 pyramidal neurons. Numbers indicate peak firing rates (Hz). Top: layout of the maze with different arms. Arrows indicate travel direction of the rat. [Color figure can be viewed in the online issue, which is available at wileyonlinelibrary.com.]

NIH-PA Author Manuscript
NIH-PA Author Manuscript
NIH-PA Author Manuscript

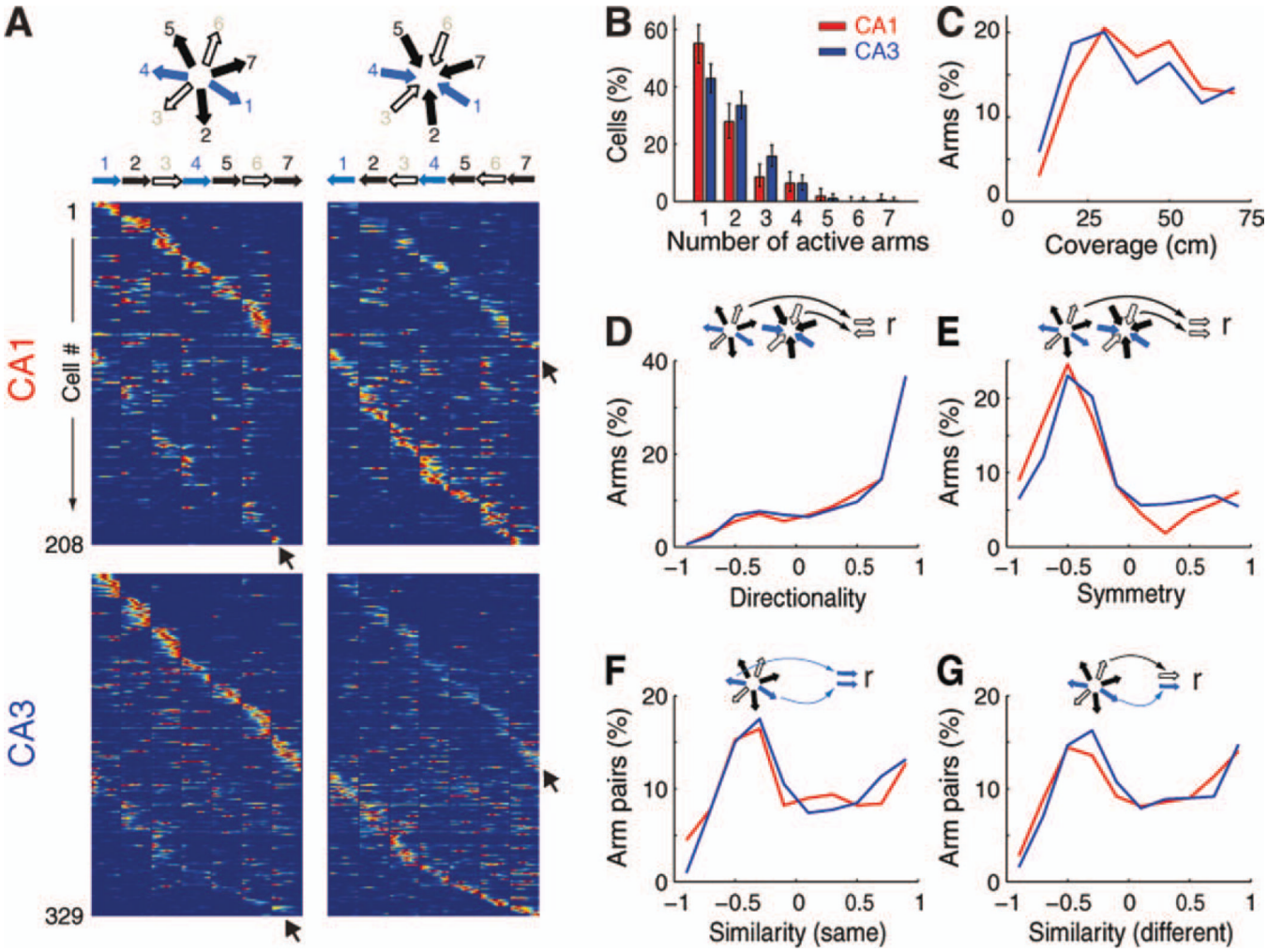

FIGURE 9.

Spatial features of CA1 and CA3 pyramidal neurons in the radial arm maze. A: The arms of the radial maze were “linearized” and concatenated. Outbound (reward) and inbound travels are shown separately (left and right panels, respectively). Black arrows indicate increased neuronal firing at place fields during opposite direction of travel. Note both neuron types were more active in the “nonpreferred” direction on the same arm on the radial maze compared with those observed on the linear track (cf. Fig. 6). B: Distribution of the number of arms with place field (±95% Clopper-Pearson confidence intervals). Active arm is an arm with peak firing rate of at least 30% of the neuron’s peak firing rate on the maze in either inbound or outbound travels. C: Coverage defined by pixels with >10% of the peak rate. D: Directionality index. E: Symmetry index. F: Similarity index (same arm type) defined as the pixel-by-pixel correlation of firing rates in the same arm types. G: Similarity index (different arm type) defined as the pixel-by-pixel correlation of firing rates in different arm types. Conventions and definitions as in Figure 7. In (D) and (E), only arms on which peak firing rate in either direction larger than 30% of the neuron’s peak firing rate on the maze are included. In (F) and (G), arm pairs at least one member of which has peak firing rate larger than 30% of the neuron’s peak firing rate on the maze are included. Red, CA1; Blue, CA3 in (B–G). [Color figure can be viewed in the online issue, which is available at wileyonlinelibrary.com.]

NIH-PA Author Manuscript

NIH-PA Author Manuscript

NIH-PA Author Manuscript

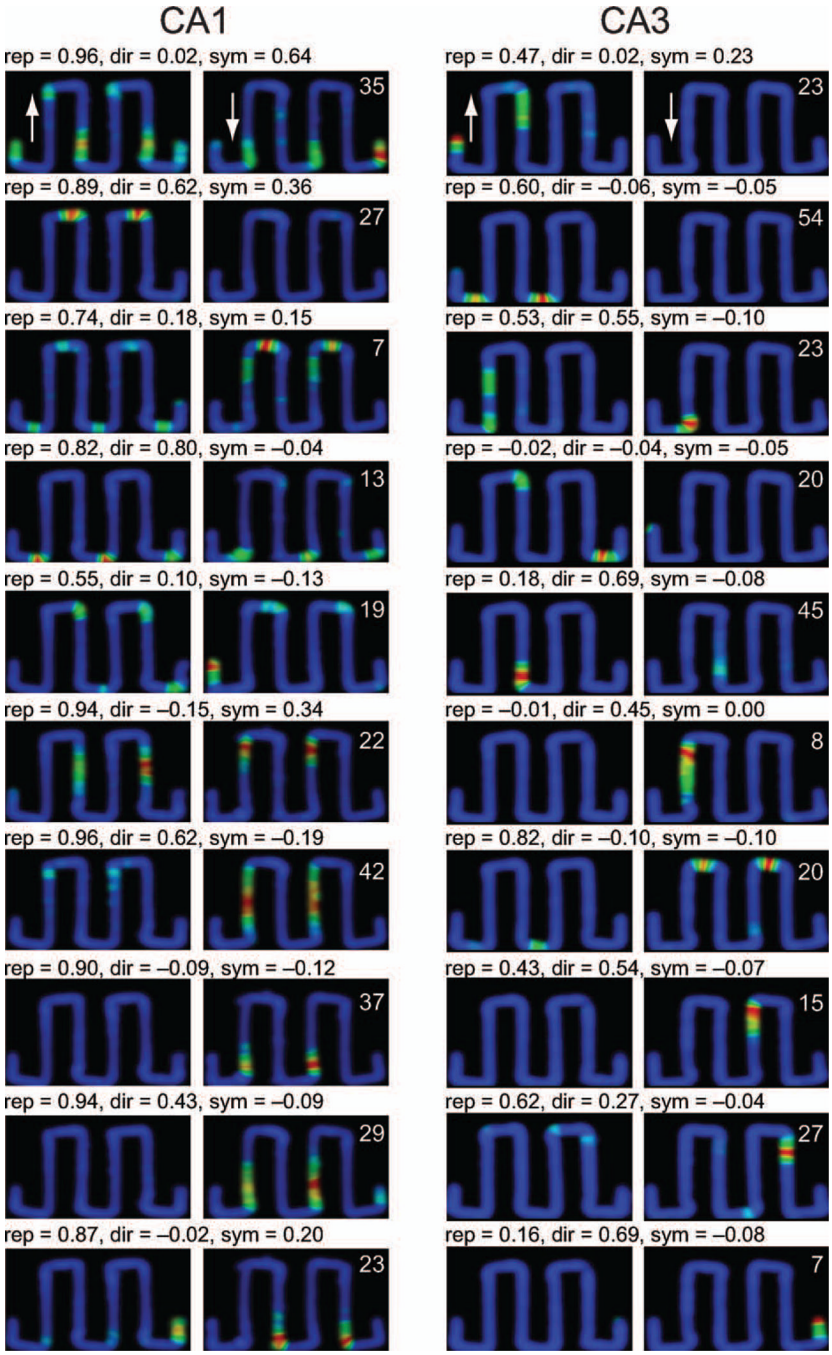

FIGURE 10.

Example place cells in the zigzag maze. Heatmaps show position-related firing rates of representative CA1 and CA3 pyramidal neurons. Numbers above plots indicate repetition index (rep), directionality index (dir), and symmetry index (sym) for each neuron. Numbers inside plots indicate peak firing rates (Hz). Note rich variability of the three indexes across individual neurons and hippocampal regions. Up and down arrows indicate right and left travels, respectively. [Color figure can be viewed in the online issue, which is available at wileyonlinelibrary.com.]

NIH-PA Author Manuscript
NIH-PA Author Manuscript
NIH-PA Author Manuscript

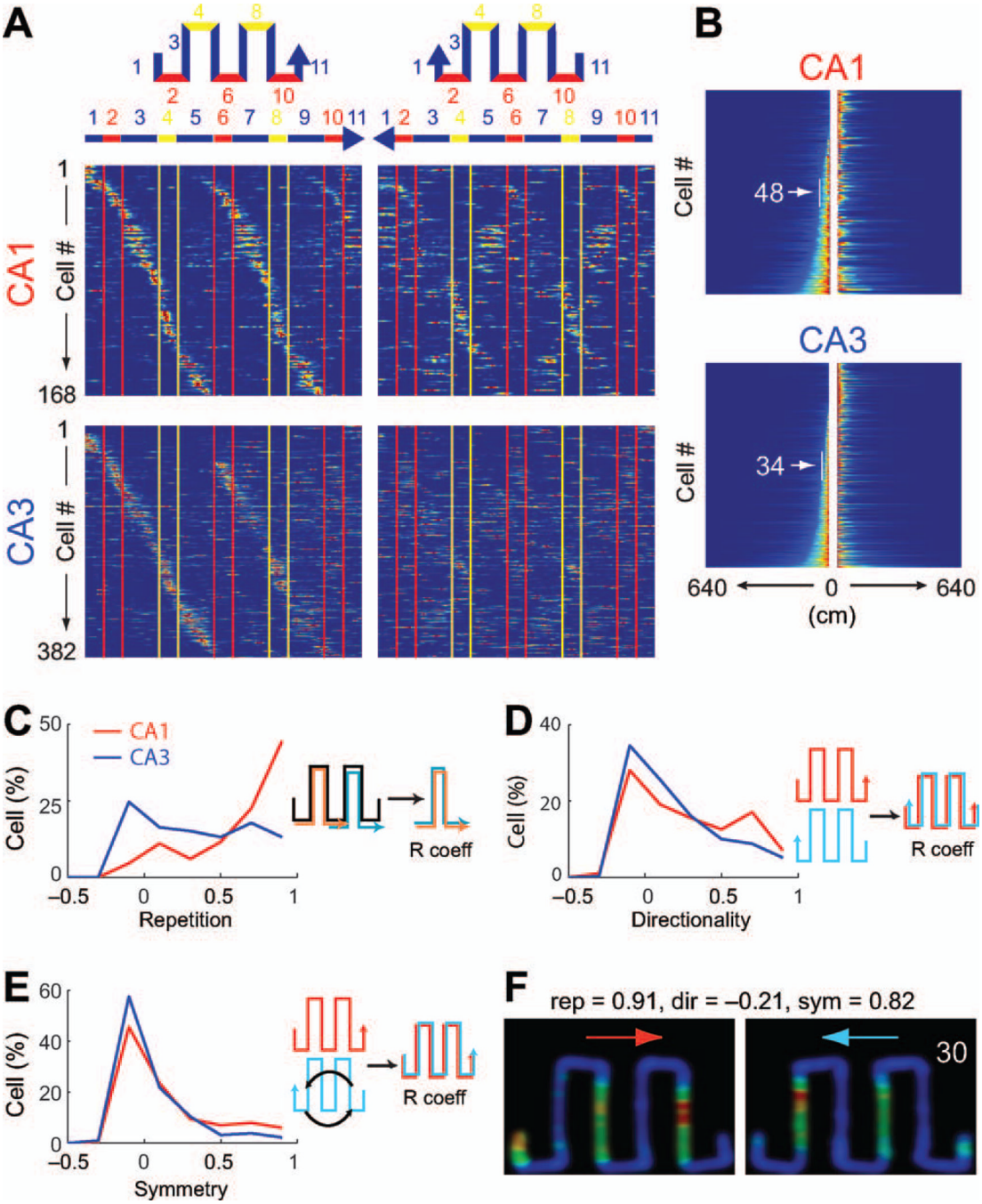

FIGURE 11.

Spatial features of CA1 and CA3 pyramidal cells in the zigzag maze. A: Color-coded, normalized firing rates of neurons in the different segments of the maze. The arms of the maze (color-coded and numbered segments) were linearized and concatenated, and neurons were ordered according to their firing field position during rightward travels (640 cm). Each horizontal line represents the same cell during rightward and leftward travels (left and right panels). Vertical lines separate respective corridors. B: Field size of CA1 and CA3 neurons during left versus right travels, ordered by field size. White arrows indicate median field size (CA1 = 48 cm, CA3 = 34 cm). C: Repetition index (R_{coeff}) between the two sets of identical corridors. Note that the majority of CA1 pyramidal cells fire at similar positions of the

repeating corridor patterns, as is also visible by two diagonal bands in (A). D: Directionality index. Note bimodal distribution of CA1 pyramidal cells. E: Symmetry index. F: An example CA1 pyramidal neuron with symmetric firing fields during left and right travels, respectively. Red, CA1; Blue, CA3 in (C–E). [Color figure can be viewed in the online issue, which is available at wileyonlinelibrary.com.]

NIH-PA Author Manuscript
NIH-PA Author Manuscript
NIH-PA Author Manuscript

NIH-PA Author Manuscript
NIH-PA Author Manuscript
NIH-PA Author Manuscript

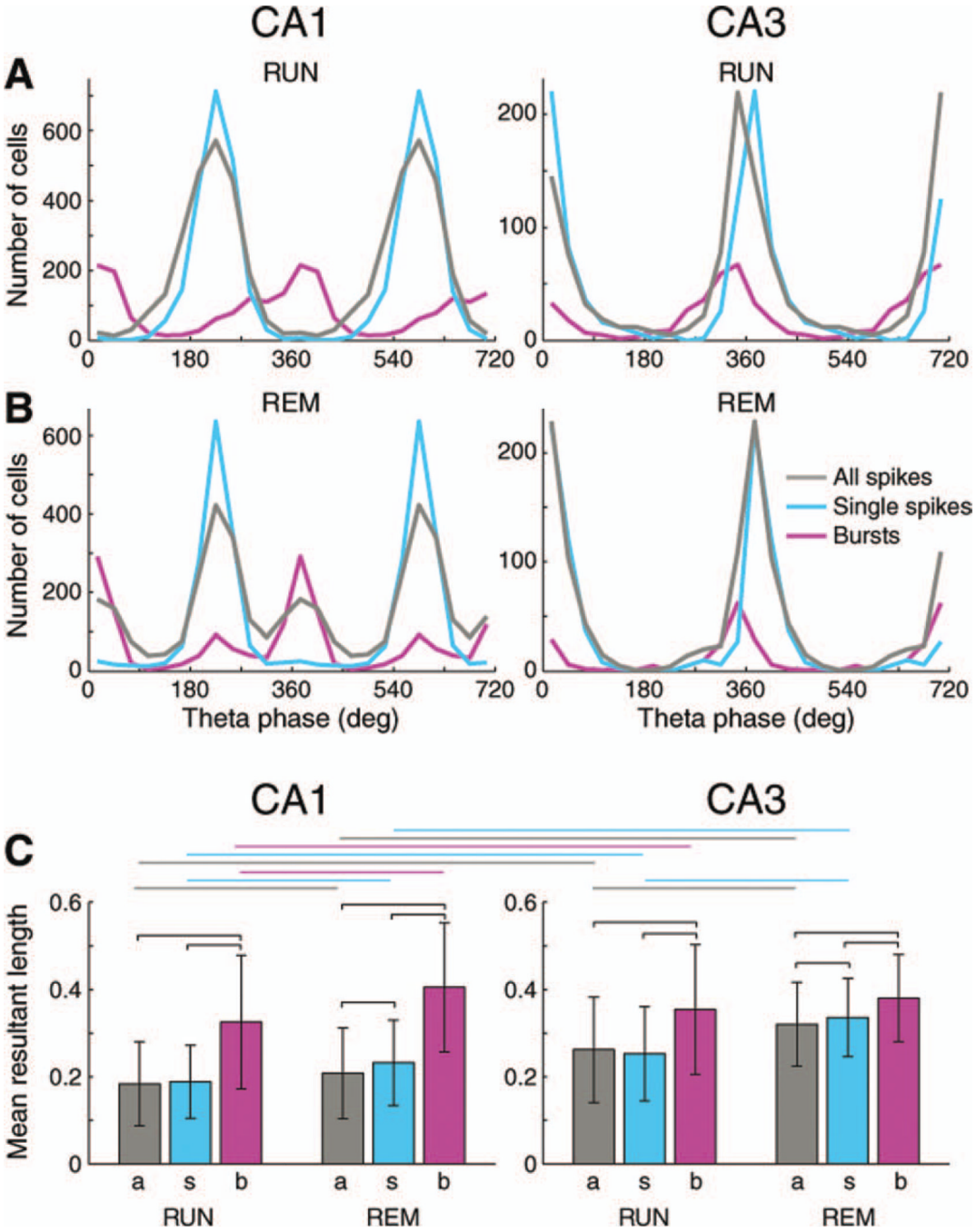

FIGURE 12.

Theta oscillation-related features of CA1 and CA3 pyramidal cells. A and B: Distribution of preferred theta phases of CA1 and CA3 pyramidal cells during RUN (A) and REM (B). Preferred phases of all spikes, single spikes (ISI > 20 ms) and bursts (three or more spikes at <6 ms intervals) are shown separately. Preferred phases refer to local (CA1 or CA3 pyramidal layer) theta. Note small phase advancement of bursts of CA3 cells relative to single spikes but large phase shift of CA1 bursts relative to single spikes. C: Magnitude of modulation depth by theta oscillation (mean resultant length ± standard deviation during RUN and REM. a, all spikes; s, single spikes; and b, bursts. Note overall stronger theta phase modulation of CA3 pyramidal cells and stronger phase-locking of bursts relative to

single spikes. All of the comparisons indicated by lines are significant ($P < 0.01$, ANOVA, followed by Tukey's honest significance test). For each ISI category, only significantly theta-modulated neurons in that category are included in (A–C). [Color figure can be viewed in the online issue, which is available at wileyonlinelibrary.com.]

NIH-PA Author Manuscript
NIH-PA Author Manuscript
NIH-PA Author Manuscript

NIH-PA Author Manuscript
NIH-PA Author Manuscript
NIH-PA Author Manuscript

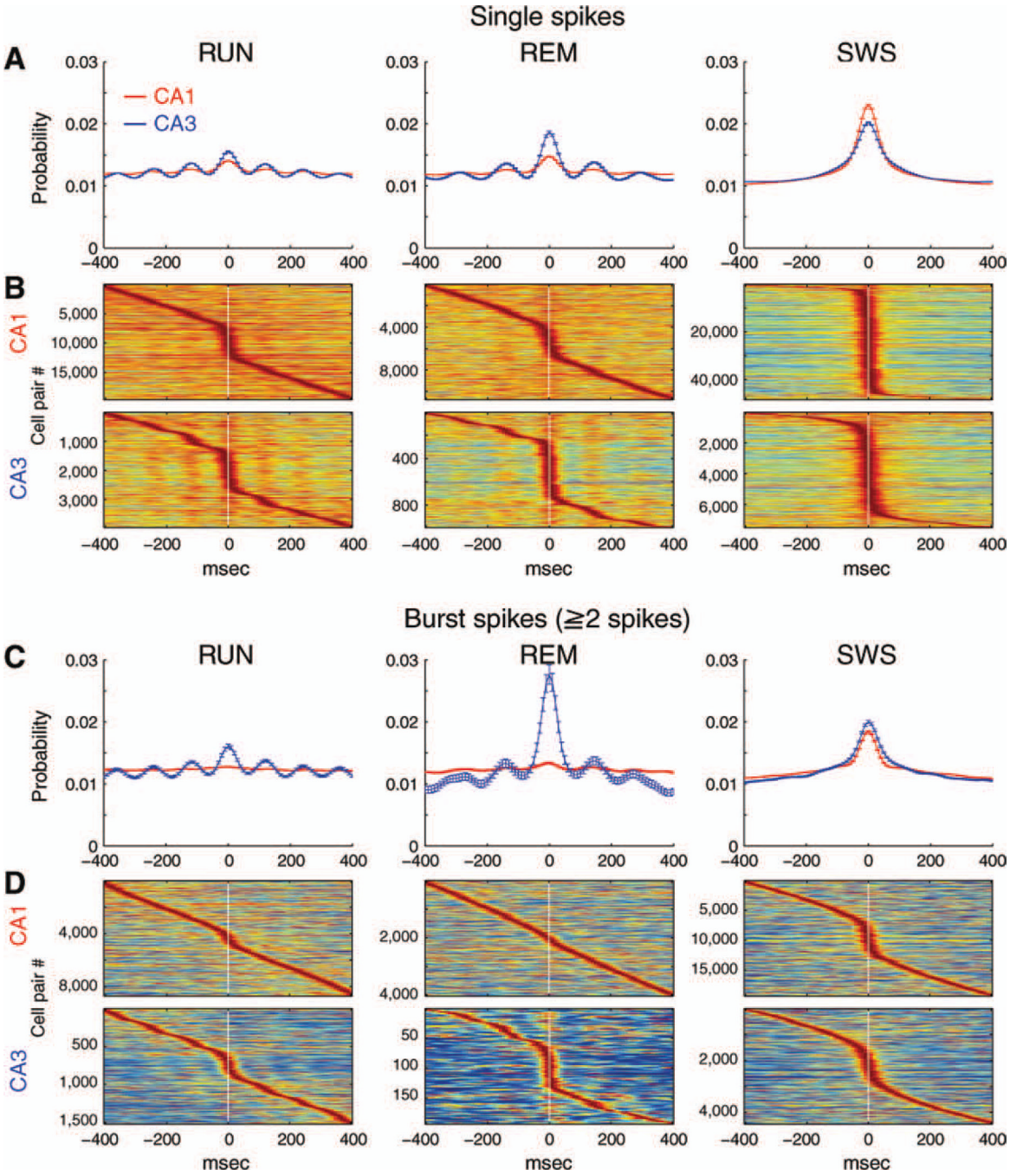

FIGURE 13.

Theta-paced cross-correlograms of CA1 and CA3 pyramidal neurons. Cross-correlograms of single spikes (ISI > 20 ms, A and B) and spikes during bursts (two or more spikes at <6 ms intervals; C and D) in different brain states. A and C: Cross-correlogram of each cell pair was first normalized so that sum of probability during −400 to 400 ms is unity, and mean ± SEM are shown. B and D: Color-coded cross-correlograms of each neuron pair. Each line is a cross-correlogram of a cell pair, normalized to it maximum value. Note stronger theta rhythmic modulation of CA3 cross-correlograms during RUN and REM, compared to CA1. Note also stronger zero-time synchrony of single spikes of CA1 but stronger synchrony of

CA3 bursts during SWS. Red, CA1; Blue, CA3 in (A) and (C). [Color figure can be viewed in the online issue, which is available at wileyonlinelibrary.com.]

NIH-PA Author Manuscript
NIH-PA Author Manuscript
NIH-PA Author Manuscript

NIH-PA Author Manuscript
NIH-PA Author Manuscript
NIH-PA Author Manuscript

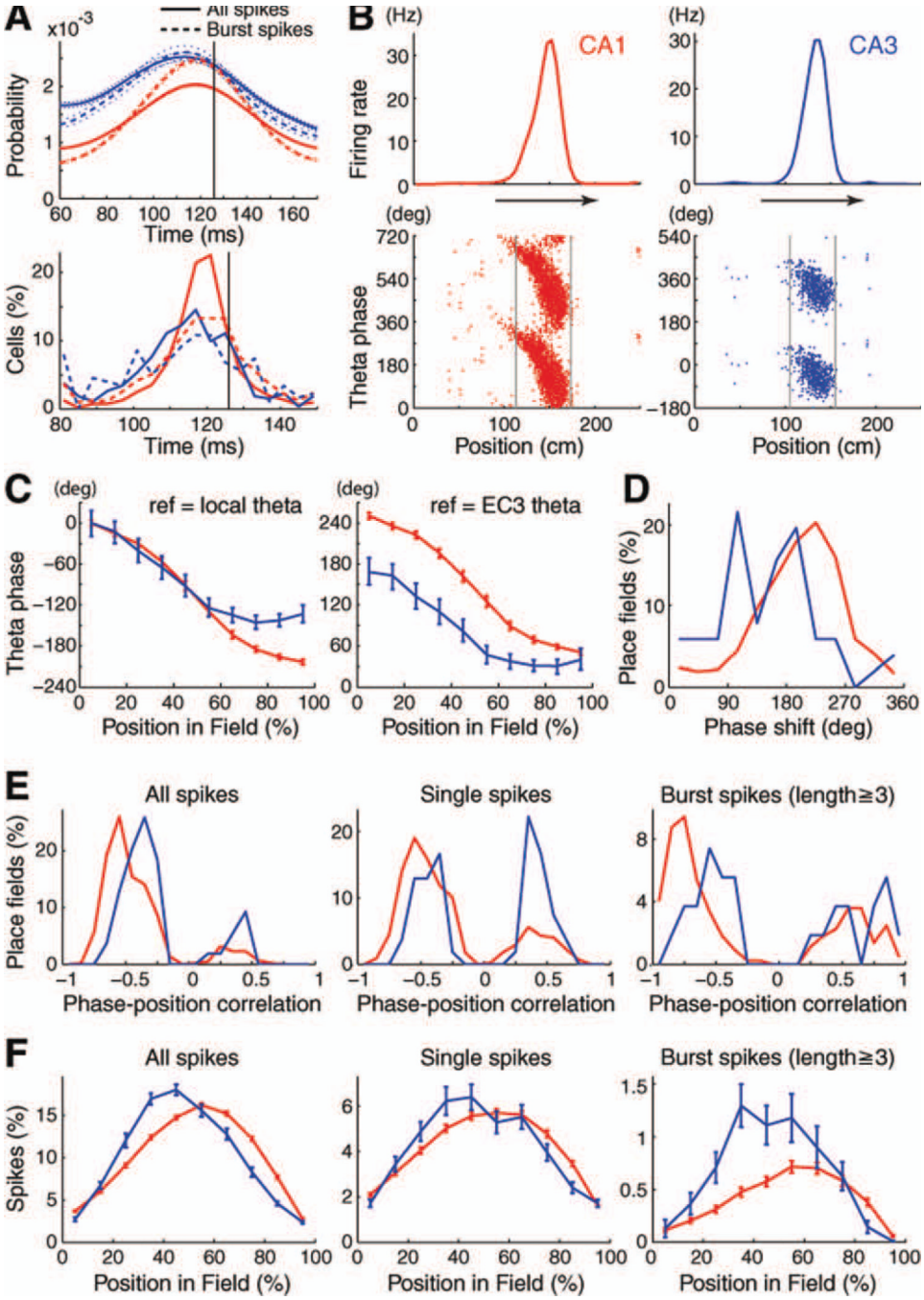

FIGURE 14.

Theta phase precession of CA1 and CA3 pyramidal cells. A: Autocorrelograms of CA1 and CA3 pyramidal cells, shown separately for all spikes (continuous line) and bursts (two spikes or more, broken lines) during walking on the linear track, zoomed to the period of theta waves. Vertical line, mean period of concurrently recorded theta waves. Mean ± SEM of autocorrelograms (top) and distribution of peaks of autocorrelograms (80–150 ms, bottom) are shown. Note significantly faster oscillation frequency of CA3 than CA1 neurons ($P < 0.0001$ for all spikes, $P < 0.001$ for burst spikes; rank sum test). B: Firing rates (top) and theta phase of spikes (bottom) as a function of the rat's position on the linear track (two theta cycles are show for clarity) for representative CA1 and CA3 pyramidal cells,

NIH-PA Author Manuscript

NIH-PA Author Manuscript

NIH-PA Author Manuscript

referenced to local LFP theta. C: Theta phase precession of spikes in CA1 (n = 798) and CA3 (n = 85) place cells with >2 Hz peak rates and >0.7 spatial coherence (Hafting et al., 2008). Mean ± 95% confident intervals are shown at 10% increments of distance from the beginning of the field on the linear track, referenced to either the local LFP theta (left) or to theta recorded from Layer 3 of the entorhinal cortex (EC3, right). 100% represents the normalized length of the place field. Note similar range of phase shift of the two populations during the inbound part of the place field, and lack of further phase precession in the outbound part in CA3 pyramidal cells. Left, for the purpose of comparison, the mean firing phases were shifted such that the mean phases of both CA1 and CA3 in the first 10% segment in the field correspond to 0°. D: Span of phase shift between the onset and offset of the place field, measured by the difference between the mean theta phase in the first 10% and the last 10% segments in the field. Note larger phase span of CA1 than CA3 neurons. E: Distribution of correlation coefficients between position and theta phase of firing, shown separately for all spikes, single spikes (>20 ms interspike intervals) and bursts (three or more spikes with <6 ms intervals). Note stronger negative phase–position correlations for CA1 neurons. F: Proportion of spikes (mean ± SEM) within the field for all spikes, single spikes (>20 ms interspike intervals) and bursts (three or more spikes with <6 ms intervals). Note asymmetric place fields for CA1 neurons, especially for bursts. Red, CA1; Blue, CA3 in all panels. [Color figure can be viewed in the online issue, which is available at wileyonlinelibrary.com.]